Endothelium-derived stromal cells contribute to hematopoietic bone marrow niche formation

Kenswil, K.J.G.; Pisterzi, P.; Sanchez Duffhues, G.; Dijk, C. van; Lolli, A.; Knuth, C.; ... ; Raaijmakers, M.H.G.P.

Cell Stem Cell

CellPress

Article

Endothelium-derived stromal cells contribute to hematopoietic bone marrow niche formation

Keane Jared Guillaume Kenswil,[1,9] Paola Pisterzi,[1,9] Gonzalo Sánchez-Duffhues,[2,9] Claire van Dijk,[1] Andrea Lolli,[3] Callie Knuth,[3] Byambasuren Vanchin,[4] Adrian Christopher Jaramillo,[1] Remco Michiel Hoogenboezem,[1] Mathijs Arnoud Sanders,[1] Jacqueline Feyen,[1] Tom Cupedo,[1] Ivan G. Costa,[5] Ronghui Li,[5] Eric Moniqué Johannes Bindels,[1] Kirsten Lodder,[2] Bianca Blom,[6] Pieter Koen Bos,[7] Marie-José Goumans,[2] Peter ten Dijke,[2,8] Eric Farrell,[3] Guido Krenning,[4] and Marc Hermanus Gerardus Petrus Raaijmakers[1,10,*]

[1]Department of Hematology, Erasmus MC Cancer Institute, Rotterdam 3015 CN, the Netherlands
[2]Department of Cell and Chemical Biology, Leiden University Medical Centre, Leiden 2300 RC, the Netherlands
[3]Department of Oral and Maxillofacial Surgery, Erasmus MC, University Medical Center Rotterdam, Rotterdam 3000 DR, the Netherlands
[4]Cardiovascular Regenerative Medicine Research Group, Department of Pathology and Medical Biology, University Medical Center Groningen, University of Groningen, Groningen 9713 GZ, the Netherlands
[5]Institute for Computational Genomics, Joint Research Center for Computational Biomedicine, RWTH Aachen, Aachen 52074, Germany
[6]Amsterdam UMC, University of Amsterdam, Department of Experimental Immunology, Amsterdam institute for Infection & Immunity, Amsterdam 1105 AZ, the Netherlands
[7]Department of Orthopaedics, Erasmus MC, Rotterdam 3015CE, the Netherlands
[8]Oncode Institute, Leiden University Medical Centre, Leiden 2300 RC, the Netherlands
[9]These authors contributed equally
[10]Lead contact
*Correspondence: m.h.g.raaijmakers@erasmusmc.nl
https://doi.org/10.1016/j.stem.2021.01.006

SUMMARY

Bone marrow stromal cells (BMSCs) play pivotal roles in tissue maintenance and regeneration. Their origins, however, remain incompletely understood. Here we identify rare LNGFR$^+$ cells in human fetal and regenerative bone marrow that co-express endothelial and stromal markers. This endothelial subpopulation displays transcriptional reprogramming consistent with endothelial-to-mesenchymal transition (EndoMT) and can generate multipotent stromal cells that reconstitute the bone marrow (BM) niche upon transplantation. Single-cell transcriptomics and lineage tracing in mice confirm robust and sustained contributions of EndoMT to bone precursor and hematopoietic niche pools. Interleukin-33 (IL-33) is overexpressed in subsets of EndoMT cells and drives this conversion process through ST2 receptor signaling. These data reveal generation of tissue-forming BMSCs from mouse and human endothelial cells and may be instructive for approaches to human tissue regeneration.

INTRODUCTION

Bone marrow stromal cells (BMSCs) contain a subset of putative adult stem cells that emerge during development and have a tissue-restricted, multilineage differentiation capacity (Bianco et al., 2008; Dominici et al., 2006). BMSCs are a heterogeneous population with putative roles in maintaining tissue homeostasis and driving regeneration of tissue after injury (Kfoury and Scadden, 2015). They play critical roles in skeletogenesis (Chan et al., 2015; Worthley et al., 2015), and they are components of the hematopoietic stem cell niche (Greenbaum et al., 2013; Méndez-Ferrer et al., 2010). The ability to expand these cells *ex vivo* and differentiate them into different lineages, together with their regenerative and immune-modulatory properties, has made them attractive candidates for exploring a potential role in regenerative medicine and tissue engineering (Brown et al., 2019).

The origin of BMSCs remains incompletely understood. The prevailing notion is that a reservoir of tissue-specific stromal stem cells is generated during development. These pools of "primordial" cells may be derived from different germ layers—i.e., the paraxial or lateral plate mesoderm (Olsen et al., 2000) and the neural crest (Isern et al., 2014; Morikawa et al., 2009a; Takashima et al., 2007)—and serve as ontogenically distinct ancestors of stromal cells with heterogeneous function in postnatal marrow (Kfoury and Scadden, 2015).

A key open question is whether the bone marrow (BM) tissue pool size of stromal cells is developmentally restricted or whether it can be modulated by *de novo* generation of BMSCs under conditions of tissue demand, such as injury. Endothelial cells (ECs) are among the first cells to reemerge in the BM after injury (Rafii et al., 2016) and orchestrate tissue development, maintenance, and regeneration by providing instructive angiocrine signals (Ramasamy et al., 2015).

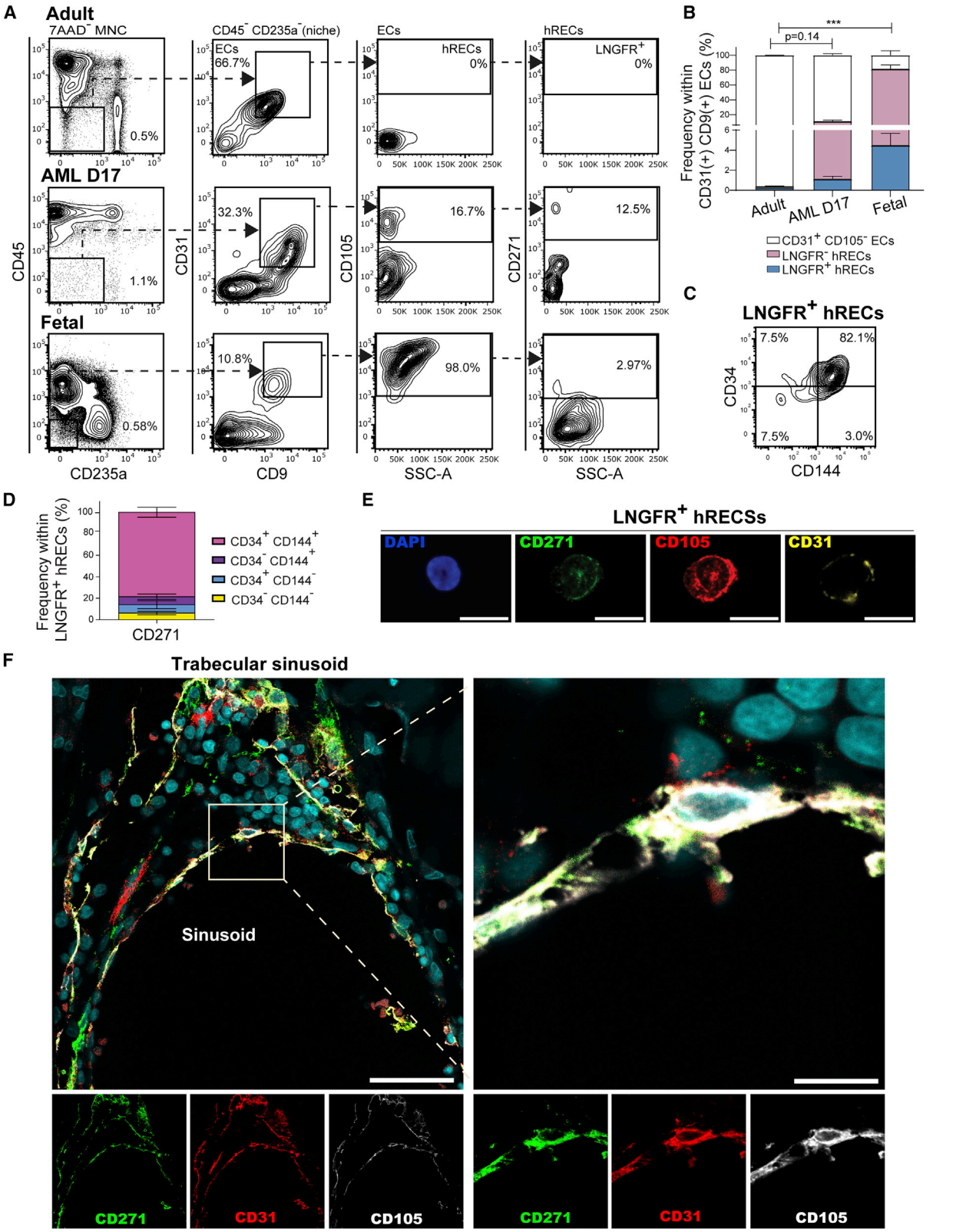

Figure 1. Identification of LNGFR-expressing human ECs in regenerative and fetal BM

(A) Flow cytometry identification of EC subsets (representative plots). A subset of ($CD45^-7AAD^-CD235^-CD31^+CD9^+CD105^+$) hRECs expresses LNGFR (CD271) upon regeneration after chemotherapy (center panels) and in fetal development (bottom panels).

(legend continued on next page)

Specific subsets of ECs that drive regeneration of bone and BM have been identified recently in mice (Kusumbe et al., 2014, 2016; Ramasamy et al., 2016), and their human counterparts are beginning to be identified. Recently, we identified human ECs associated with BM regeneration and development (Kenswil et al., 2018). These endoglin (CD105)-expressing ECs, dubbed $CD31^+CD9^+CD105^+$ human regeneration-associated ECs (or hRECs), constitute a fraction of ECs, emerging during fetal development and regeneration after chemotherapy (conditions under which angiogenesis, hematopoiesis, and osteogenesis are tightly coupled) with a distinct transcriptional landscape (Kenswil et al., 2018).

ECs can be coerced *ex vivo* toward stromal cell types through a process of transdifferentiation called endothelial-to-mesenchymal transition (EndoMT) (Dejana et al., 2017; Piera-Velazquez and Jimenez, 2019; Sanchez-Duffhues et al., 2016), but the relevance of this process for human BM development remains unknown.

Here we identify an EC-derived cell type in human BM that appears under conditions requiring tissue formation with the capacity to generate skeletal stem-like BMSCs able to reconstitute the entire hematopoietic niche *in vivo*. Lineage tracing experiments in mice confirm a robust contribution of these specialized, endothelium-derived stromal cells (eBMSCs) to the hematopoietic BM niche. Interleukin-33 (IL-33) is identified as a novel factor driving the conversion of human ECs to such "stroma-primed" ECs.

RESULTS

Identification of rare LNGFR-expressing human ECs in regenerative and fetal BM

We recently characterized a distinct subset of CD105 $(endoglin)^+$ ECs emerging during human fetal development and BM regeneration after injury (hRECs) (Kenswil et al., 2018). Interrogation of the transcriptome of these ECs revealed expression of transcripts typically associated with stromal cell fates, including *THY1* (CD90) and *NGFR* (CD271) (Table S1), suggesting the possibility that a subset of hRECs with stromal properties might exist during human fetal development.

Protein expression of LNGFR (CD271), a well-established marker of primary human BM stromal cells (Jones et al., 2010; Quirici et al., 2002; Tormin et al., 2011) encoded by the *NGFR* gene, was confirmed in a subset of fetal hRECs by flow cytometry (Figures 1A and 1B). This subset of LNGFR-expressing hRECs was virtually absent in human adult BM under steady-state conditions (isolated from healthy BM donors; 0.27% ± 0.1% of $CD31^+CD9^+$ ECs) but highly enriched in human fetal BM (gestational weeks 15–20; 4.47% ± 1.2% of $CD31^+CD9^+$ ECs; one-way ANOVA [$p < 0.0001$] followed by Bonferroni's multiple comparisons test [$p = 0.001$]) and human BM upon recovery following chemotherapy injury (17 days after start of chemotherapy for acute myeloid leukemia [AML]; Kenswil et al., 2018; 1.11% ± 0.3% of the $CD31^+CD9^+$ EC population, Bonferroni's multiple comparisons test [$p = 0.14$]). In addition, $LNGFR^+$ hRECs expressed other *bona fide* markers of endothelium, such as CD34 and CD144 (VE-cadherin) (Figures 1C and 1D), stressing their endothelial identity. To exclude the possibility that co-expression of endothelial and stromal markers reflects close proximity of two cells (identified as a single event in flow cytometry despite "doublet" exclusion), $LNGFR^+$ hRECs were sorted by fluorescence-activated cell sorting (FACS), and co-expression of CD31, CD105, and LNGFR was confirmed at the single-cell level by immunocytochemistry (Figures 1E and S1C–S1E).

Previously, we showed that hRECs are enriched in collagenase-treated human bone fractions (Kenswil et al., 2018). $LNGFR^+$ cells were identified in this hREC fraction in collagenased adult bone (obtained from individuals undergoing hip replacement surgery; 2.7% ± 0.7% of $CD31^+CD9^+$ ECs) and fetal bone fractions (4.1% ± 1.0% of $CD31^+CD9^+$ ECs) (Figures S1A and S1B).

Confocal imaging of human fetal bones revealed the presence of $CD31^{+(dim)}$ $CD271(LNGFR)^+CD105^+$ cells in blood vessels, in particular ECs aligning sinusoids localized in trabecular areas (Figures 1F and S1F). $CD271^+$ ECs seemed less abundant in sinusoids in medullar areas of fetal bone and were not observed in arterial/arteriolar ($CD31^{high}$) structures (Figure S1G).

These data demonstrate that a rare subtype of $LNGFR^+$ ECs exists in human bone and marrow that is highly enriched in frequency during development and regeneration.

LNGFR-expressing ECs display a transcriptional signature of cells undergoing endothelial-to-mesenchymal transition

We next hypothesized that this rare cell type, co-expressing endothelial and stromal markers, might reflect ECs undergoing EndoMT; that is, the transition of endothelial to stromal cell fates, characterized by downregulation of endothelial makers and increased expression of stromal markers (Dejana et al., 2017; Piera-Velazquez and Jimenez, 2019; Souilhol et al., 2018).

To begin addressing in more detail whether $LNGFR^+$ ECs fulfill this criterion, we interrogated, by massive parallel RNA sequencing, the transcriptome of highly FACS-purified $LNGFR^+$ hRECs in comparison with other endothelial ($LNGFR^-$ hRECs) and stromal ($CD31^-LNGFR^+$ stromal cells) subsets sorted from

(B) EC subset frequencies in adult steady-state (n = 13), regenerative (n = 48), and fetal BM (n = 15). ***$p < 0.001$, one-way ANOVA ($p < 0.0001$) followed by Bonferroni's multiple comparison test.
(C and D) Expression of the endothelial markers CD34 and CD144 in fetal BM $LNGFR^+$ ECs. Shown are (C) a representative flow plot and (D) frequencies (n = 13).
(E) Cropped immunofluorescence image confirming cell surface expression of CD31, CD105, and CD271 on FACS-sorted $LNGFR^+$ hRECs. The white scale bar represents 10 μm.
(F) Representative confocal image of human fetal bone, demonstrating the localization of $CD31^+CD271^+CD105^+$ ECs in sinusoidal vessels of the trabecular area (left panel, 63× magnification). A magnified inset is shown in the right panel. DAPI stained nuclei are represented in blue. Scale bars, 50 μm (left panel) and 5 μm (right panel).
See also Figure S1 and Table S1.

the same BM samples. Hierarchical clustering by principal-component analysis of transcriptomes revealed strikingly separate clustering of the sorted endothelial and stromal populations (Figure 2A). The transcriptome of LNGFR$^+$ hRECs clustered between those of LNGFR$^-$ hRECs and CD31$^-$LNGFR$^+$ stromal cells.

Transcript analysis confirmed robust expression of multiple *bona fide* markers of ECs in LNGFR$^+$ hRECs, including *PECAM1*, *CDH5* (encoding CD144/VE-cadherin), and others (Figure 2B). Expression of *PECAM1* (CD31) and other endothelial markers was consistently lower in LNGFR$^+$ hRECs in comparison with LNGFR$^-$ hRECs, in line with the finding of reduced CD31 protein expression by immunocytochemistry (Figures 1 and S1C). In addition to reduced expression of endothelial markers, LNGFR$^+$ hRECs displayed increased expression of multiple markers typically associated with primitive stromal cells, such as *LEPR* and *PDGFRA* (CD140a) (Figure 2C), at levels comparable with those of stromal BM cells. Genes encoding markers of bone progenitor cells were highly or uniquely overexpressed in LNGFR$^+$ hRECs in comparison with LNGFR$^-$ hRECs (Figure 2D).

Importantly, the distinct expression of endothelial markers confirms their endothelial nature and clearly separates these cells from perivascular stromal cells/pericytes, which lack expression of these endothelial markers (Crisan et al., 2008).

The unique transcriptional feature of reduced expression of endothelial markers concomitant with activation of stromal programs suggests that LNGFR$^+$ hRECs may reflect ECs undergoing EndoMT.

Further supporting this notion, analysis of transcriptional programs by gene set enrichment analysis (GSEA) revealed remarkable enrichment of transcriptional signatures associated with transition to stromal cell fates in LNGFR$^+$ hRECs in comparison with LNGFR$^-$ hRECs (Figures 2E and S2A). Similarly, Gene Ontology (GO) term analysis revealed biological programs related to stromal cells in LNGFR$^+$ hRECs, including extracellular matrix production and ossification (Table S2).

Gene sets associated with signaling pathways shown previously to regulate epithelial-to-mesenchymal transition (EMT) as well as EndoMT, including the transforming growth factor β (TGF-β) (Azhar et al., 2009), fibroblast growth factor (FGF) (Lee et al., 2004), Hedgehog (Syn et al., 2009), and WNT (Hurlstone et al., 2003) signaling pathways, were significantly enriched in LNGFR$^+$ hRECs (Figures S2B–S2E). These signaling pathways have been shown to activate the transcription factors driving EndoMT (Pardali et al., 2017), including members of the Snail (Kokudo et al., 2008; Mahmoud et al., 2017), Twist (Ansieau et al., 2008; Chakraborty et al., 2010), and ZEB (Bracken et al., 2008) transcription factor families. Strikingly, many of these key transcription factors driving EndoMT (*SNAI2* [Slug], *TWIST1*, *TWIST2*, *YAP1*, and *ZEB2)* were overexpressed in LNGFR$^+$ hRECs compared with LNGFR$^-$ hRECs (Figure 2F). This simultaneous overexpression of transcriptional mediators has been described previously as an important feature of ECs undergoing EndoMT (Wesseling et al., 2018).

These data indicate that LNGFR$^+$ hRECs exhibit molecular characteristics congruent with ECs undergoing mesenchymal transition and might be capable of giving rise to primitive stromal cells and their downstream differentiated progeny.

LNGFR$^+$ ECs display transcriptional features of stemness and give rise to stromal progenitors with multilineage differentiation capacity

Conversion of vascular ECs into stromal cells has been demonstrated previously *in vivo* during embryonic development (Eisenberg and Markwald, 1995; Markwald et al., 1975). However, whether primary ECs with this capacity exist in human BM and contribute to human tissue formation has remained unknown. Acquisition of stem-cell-associated and developmental transcriptional programs in LNGFR$^+$ hRECs was suggested by GSEA and GO analysis (Figure S2F; Table S2). GO term analysis further revealed enrichment of gene sets associated with skeletal and neuronal development (Table S2), suggesting that LNGFR$^+$ hRECs might have the potential to contribute to skeletogenesis.

LNGFR$^+$ hRECs, when cultured in endothelium-supporting medium, spontaneously formed a stromal layer of cells morphologically resembling fibroblasts after 6–7 days of culture (Figure S3A). Flow cytometry analyses of these stromal cells revealed robust expression of markers associated with cultured multipotent stromal cells (Dominici et al., 2006), including CD105, CD73, CD90, CD51, and CD146 (Figure S3B), with loss of endothelial markers (CD34 and CD31) (Figure S3C).

The ability to form stromal colonies (CFU-F capacity) was restricted to LNGFR$^+$ hRECs and not found in other endothelial subsets (Table S3). Single-cell sorting of freshly isolated cells revealed the frequency of cells with CFU-F formation capacity among LNGFR$^+$ hRECs to be 1 in 10 ± 0.1 in comparison with 1 in 6 ± 1.5 of CD31$^-$ LNGFR$^+$ stromal cells (Figure S3D). eBMSCs were able to expand extensively, demonstrated extensive serial replating capacity (performed until 15 passages without signs of exhaustion; data not shown), and had the capacity to be differentiated into osteoblastic, chondrogenic, and adipocytic cells under defined culture conditions (Figure S3E).

The vast majority of LNGFR$^+$ hRECs (>80%) expresses CD144 (*CDH5*) as a *bona fide* and specific marker of ECs (Figures 1C and S3F). To further confirm that this subset of ECs can give rise to stromal progenitor cells, sorting and *ex vivo* culture of the CD144$^+$LNGFR$^+$ hREC population was performed (Figure S3F), which demonstrated that this particular endothelial subset harbors cells with the ability to form stromal cells with serial replating (Figure S3G) and multilineage differentiation capacity (Figure S3H). These *ex vivo* stromal progenitors lacked protein expression of markers typical for hematopoietic cells and ECs (CD45, CD34, CD31, and CD144; Figure S3I) and expressed markers associated with cultured stromal cells (CD105, CD73, CD90, and CD146; Figure S3J).

Finally, eBMSCs were able to support hematopoietic stem/progenitor cells (HSPCs) (Figures S4A and S4B). Co-culture of umbilical cord blood (UCB)-derived CD34$^+$ HSPCs resulted in expansion of these cells to the level of CD31$^-$ LNGFR$^+$ stromal cells, which have been shown previously to support expansion of HSPCs (Li et al., 2014). The capacity to support hematopoiesis coincided with high expression of hematopoietic stem cell (HSC)-regulating genes such as *VCAM1*, *SELE* and *CXCL12*, and *ANGPT1* (Figure S4C).

These data demonstrate that LNGFR$^+$ hRECs have the capacity to convert to stromal stem cell-like cells with expression of stem cell transcriptional signatures, the ability to form CFU-F with serial replating ability, and multilineage differentiation

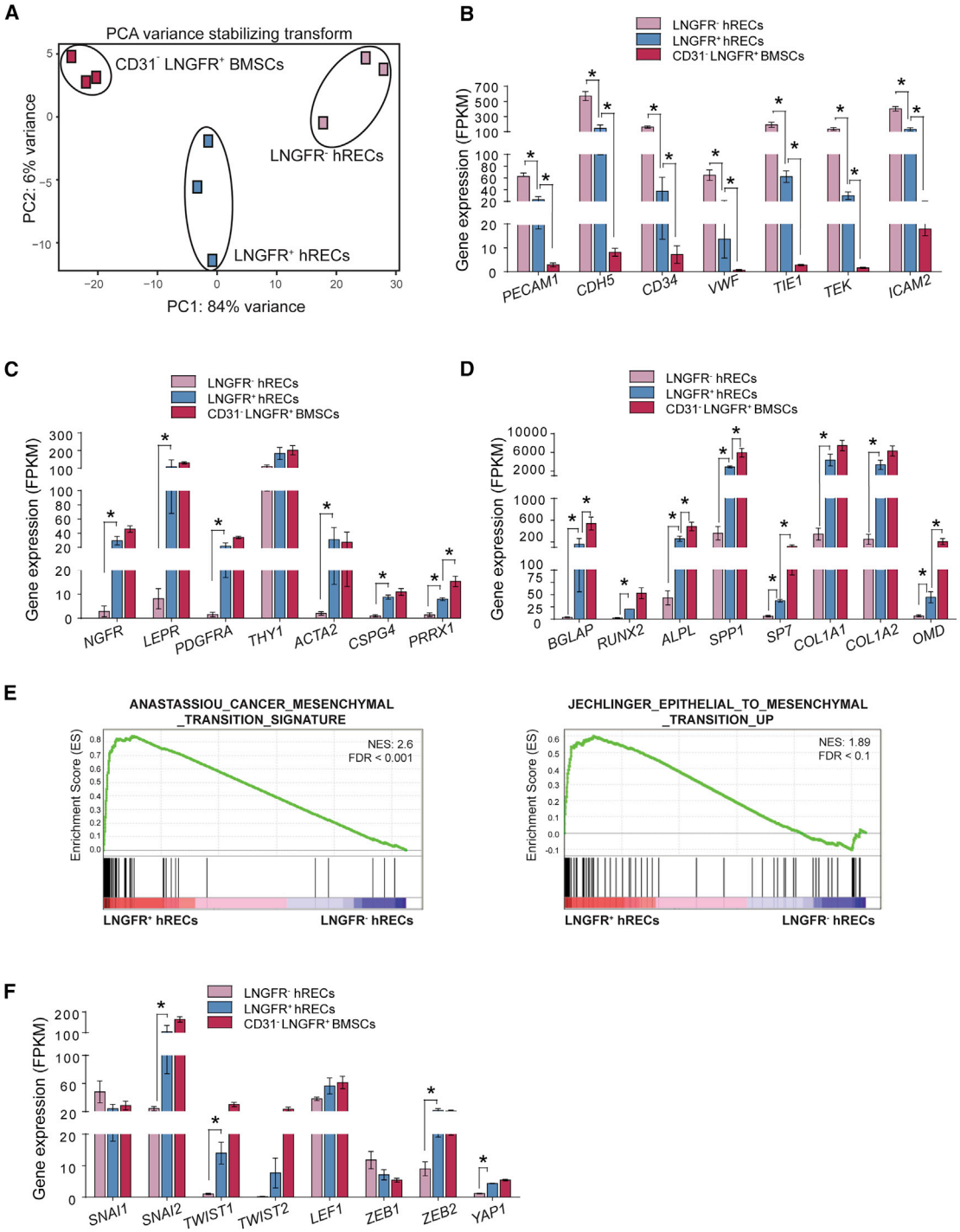

Figure 2. LNGFR⁺ ECs exhibit transcriptional characteristics of cells undergoing mesenchymal transition

LNGFR⁺ hRECs display reduced expression of endothelial genes and increased expression of stromal genes and transcription factors driving EndoMT in comparison with LNGFR⁻ hRECs.

(A) Principal-component analysis (PCA) revealing distinct hierarchical clustering of cell populations.

(B and D) Expression of genes encoding for endothelial markers (B), stromal markers (C), and osteolineage markers (D).

(E) Activation of transcriptional programs (see also Figure S2A) associated with mesenchymal transition in LNGFR⁺ hRECs.

(F) Expression of genes encoding for known EndoMT drivers.

Data are from 3 human fetal bones. *false dicovery rate (FDR) < 0.05. FPKM, fragments per kilobase of exon per million fragments mapped; NES, normalized enrichment score.

See also Figure S2 and Table S2.

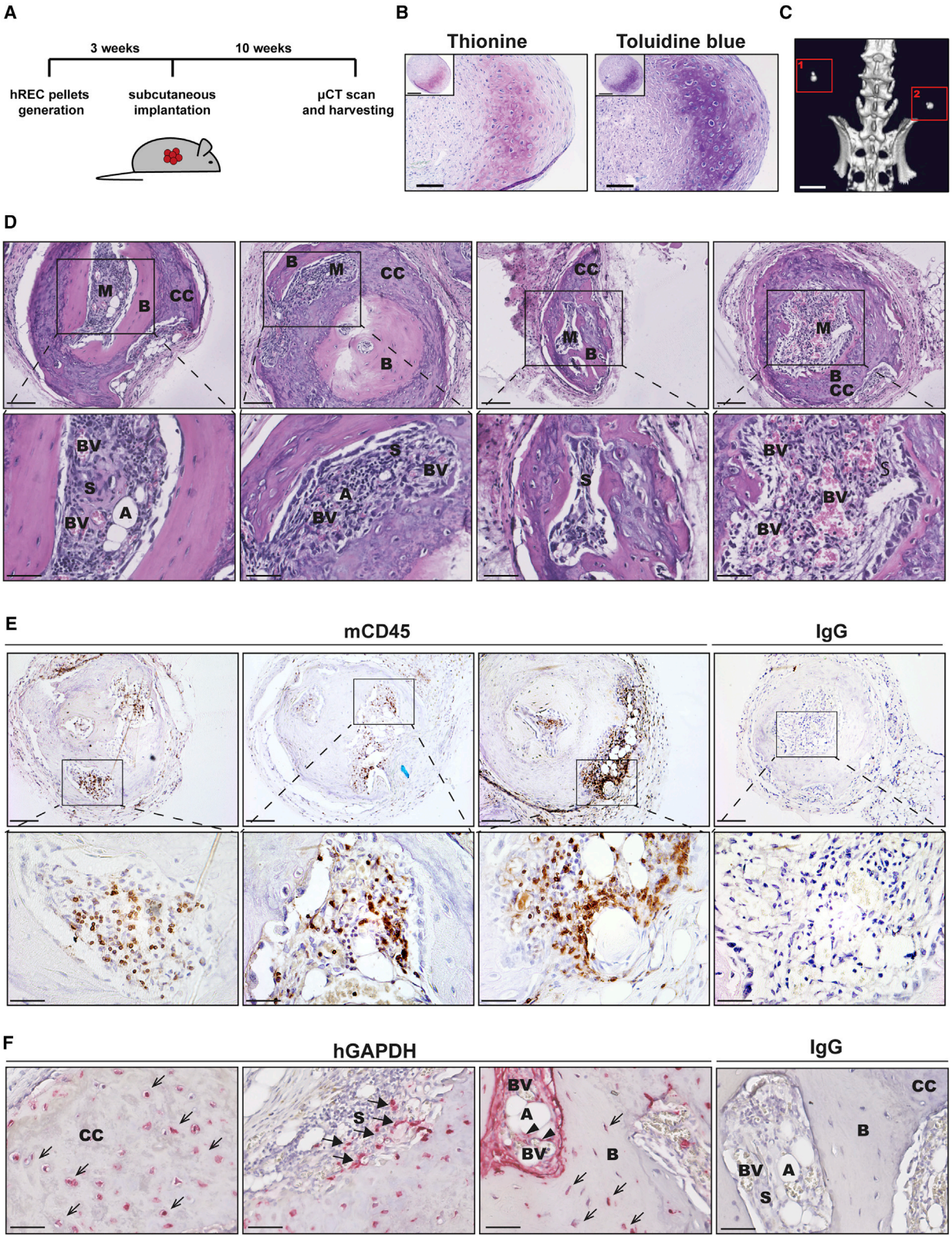

Figure 3. eBMSCs have *in vivo* hematopoietic niche establishment capacity

(A) Stromal cells derived from LNGFR$^+$ ECs (eBMSCs) were induced to form 3D pellets and subjected to 3 weeks of culture in chondrogenic medium prior to subcutaneous implantation in athymic nude mice. 10 weeks post-implantation, pellet mineralization was assessed by μCT analysis, and the constructs were retrieved for histological processing. Representative data of 6 transplanted constructs are shown.

(legend continued on next page)

capacity. These cells may thus be hypothesized to have the potential to contribute to BM development by transdifferentiation into bone lineages and by providing support for nascent hematopoiesis.

Human eBMSCs form an *in vivo* BM niche

The ability of LNGFR$^+$ ECs to generate stromal cells with skeletal differentiation and hematopoiesis support capacity *in vitro* suggests that they may represent *bona fide*, *in vivo*, hematopoietic niche (re)generating cells. Such cells have been defined previously as skeletal stem cells (SSCs), clonogenic skeletal progenitors capable of establishing the hematopoietic microenvironment (Sacchetti et al., 2007). To test whether eBMSCs contain SSCs, we exploited a previously established protocol of human BMSC cultured as 3D pellets under chondrogenic priming conditions, followed by subcutaneous implantation in mice (Farrell et al., 2011; Scotti et al., 2013; Serafini et al., 2014). eBMSCs obtained from fetal bone were subjected to chondrogenic differentiation as 3D pellets for 3 weeks (Figure 3A). This resulted in 3D cartilage pellet formation, as shown by glycosaminoglycan production (toluidine blue and thionine staining; Figure 3B). Subsequently, pellets were implanted subcutaneously into recipient mice (6 pellets/pocket). After 10 weeks, micro-computed tomography (μCT) scans demonstrated mineralization of the pellets (Figure 3C). Following harvest of the pellets, histological analyses revealed heterotopic ossicle formation in all harvested pellets with the presence of bone, cartilage, adipocytes, blood vessels, and hematopoietic tissue (Figure 3D). The presence of hematopoietic tissue was further confirmed by staining with the pan-hematopoietic marker CD45 (Figures 3E and S4F for mouse BM positive control) and the presence of megakaryocytes (Figure S4G). Human origin of osteocytes, chondrocytes, BMSCs, and adipocytes was confirmed by immunohistochemistry using an antibody against human-specific glyceraldehyde 3-phosphate dehydrogenase (GAPDH) (Figures 3F, S4H, and S4I).

The transplantation data establish the *in vivo* multi-lineage skeletogenic differentiation and hematopoietic niche formation capacity of the LNGFR$^+$ EC-derived stromal cell population.

Identification of EndoMT cells by single-cell transcriptomics (single-cell RNA sequencing [scRNA-seq]) during BM development in mice

Identification of eBMSCs with hematopoietic niche formation capacity raises the question whether such cells represent mesodermal precursors of endothelial and stromal cells (mesenchymo-angioblasts) (Bianco and Cossu, 1999; Cossu and Bianco, 2003; Slukvin and Kumar, 2018) or are a result of ECs undergoing EndoMT in human BM. The transcriptional landscape of LNGFR$^+$ ECs, including expression of EndoMT-driving transcription factors, strongly suggests the latter possibility. To formally demonstrate that eBMSCs contribute to the hematopoietic niche in mammalian development, single-cell transcriptomics (scRNA-seq) and lineage tracing (see eBMSCs contribute to BM tissue and niche formation in mice) were performed in mice.

BMSCs (CD45$^-$Ter119$^-$CD31$^-$CD51$^+$Sca$^+$; Morikawa et al., 2009b; Pinho et al., 2013; Schepers et al., 2012) and ECs (CD31$^+$, including VE-cadherin$^+$ cells) were FACS-purified from BM and collagenased bone fractions of the long bones of mouse fetuses at embryonic day 17 (E17) (Figure 4A). At E17, the BM cavity is being vascularized, osteoblast formation and calcification occurs, and hematopoiesis shifts from the fetal liver to the BM, with the first fetal BM HSPC activity being detected at E16.5 (Coşkun et al., 2014), reflecting the developmental stage examined in humans (Figures 1 and 2).

scRNA-seq of pooled BMSC and EC fractions (of 9 fetuses) revealed two distinct clusters (Figure 4B), separating ECs (*Cdh5*$^+$, *Pecam1*$^+$) from stromal elements (*Prrx1*$^+$, *Col1a1*$^+$) (Figure 4B). Endoglin (*Eng*) was expressed in the majority of ECs (Figure 4B), in line with our findings regarding human fetal development (Figure 1), whereas *Ngfr* expression was restricted to a subset of cells, predominantly in the stromal population (Figure 4B).

Although the vast majority of cells expressing endothelial markers (*Cdh5* and *Pecam1*) were found in the endothelial cluster, some of these cells were located in the stromal cluster. Conversely, a minority of cells in the "endothelial" cluster expressed stromal markers (*Prrx1*$^+$, *Col1a1*$^+$, and *Pdgfra*$^+$), opening the possibility of the existence of a "transitional" population expressing *bona fide* endothelial and stromal transcripts. Indeed, separate re-clustering of all cells expressing the endothelial marker *Cdh5* (Figure 4C) identified a distinct subset of cells that was characterized by co-expression of endothelial transcripts (*Cdh5*, *Pecam1*, and *Eng*), stromal transcripts (*Col1a1* and *Prrx1*), and transcription factors involved in EndoMT regulation (*Snai2*, *Twist1*, and *Zeb2*) (Figure 4D), which included cells expressing *Ngfr* (Figure 4E). Quantitation of transcripts in this cluster, in comparison with the other clusters in the *Cdh5*-expressing endothelial population (Figure 4F), revealed reduced expression of endothelial markers (*Cdh5*, *Pecam1*, and *Eng*) with concomitantly increased expression of stromal markers (*Col1a1*, *Prrx1*, *Fap*, and *Cspg4*(*Ng2*)), EndoMT transcription factors (*Twist1* and *Zeb2*), and the HSPC mobilizing factor *Cxcl12*, indicative of cells undergoing EndoMT (Piera-Velazquez and Jimenez, 2019).

This notion was corroborated by striking enrichment of gene sets reflecting EMT (Figure 4D, inset; normalized enrichment

(B) Glycosaminoglycan production in 3D pellets at the time of implantation (day 21), as shown by thionine and toluidine blue staining. Scale bars, 100 μm (inset) and 200 μm.
(C) Representative 3D reconstruction from μCT scans of implanted pellets. Scale bar, 3 mm.
(D–F) Representative microphotographs of histological sections of bone constructs.
(D) Hematoxylin and eosin staining demonstrating bone and hematopoietic niche formation (high-magnification insets). Scale bars, 100 μm and 50 μm (insets).
(E) Mouse CD45 (mCD45) staining confirming the presence of hematopoietic cells in the marrow. An isotype immunoglobulin G (IgG) antibody was used as negative control for the staining. Scale bars, 100 μm and 50 μm (insets).
(F) Human-specific GAPDH (hGAPDH) detecting human cells in the calcified cartilage (CC) and bone (B) (open arrow) as well as in the BM (M), stroma (S) (closed arrow), and adipose tissue (A) (black arrowhead), indicating the presence of donor LNGFR$^+$ EC-derived cells in the various BM compartments. An isotype IgG monoclonal antibody was used as negative control for the staining. Scale bars, 50 μm. BV, blood vessel.
See also Figures S3 and S4 and Table S3.

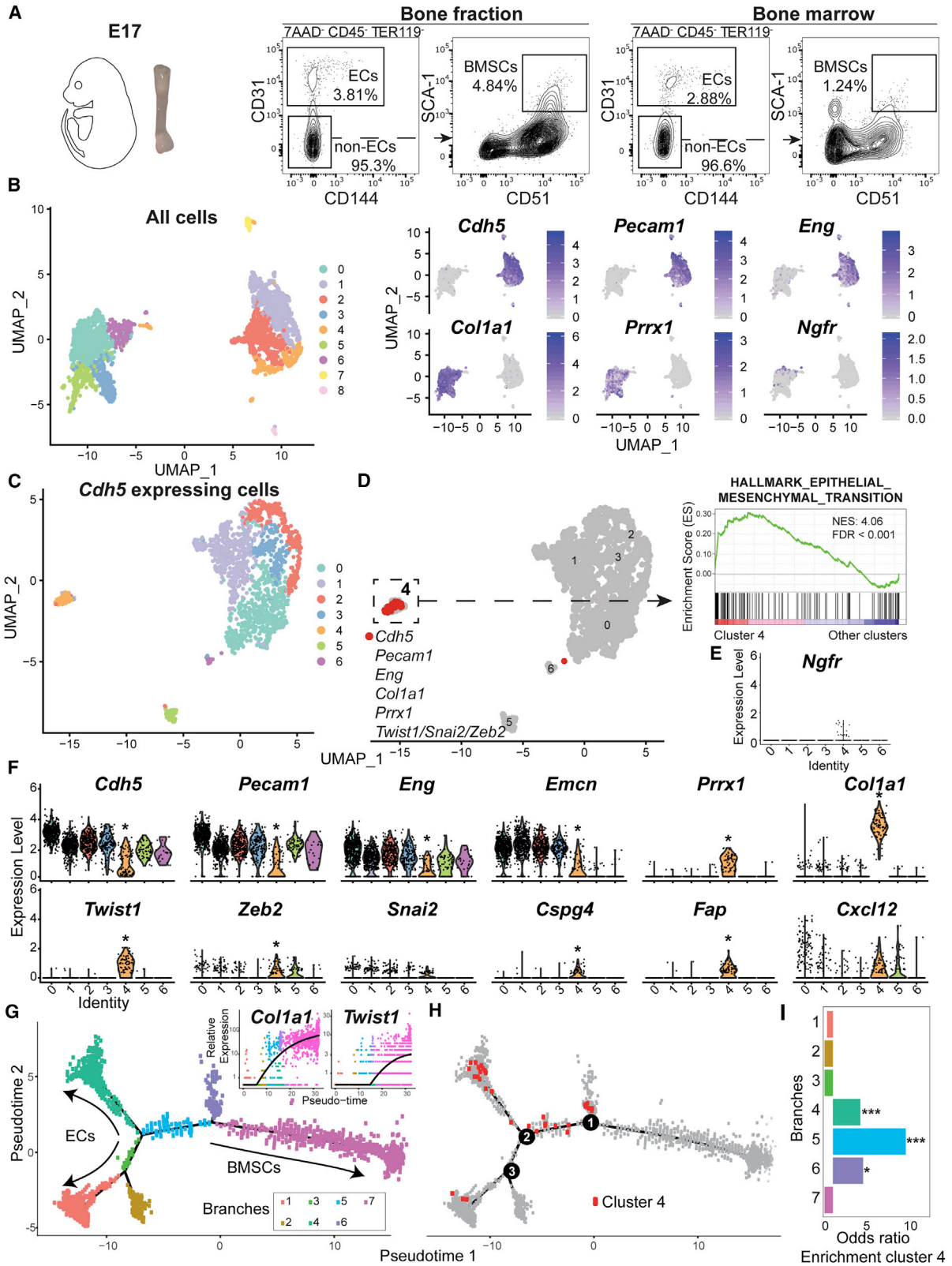

Figure 4. Identification of EndoMT cells by scRNA-seq during BM development in mice

(A) Flow cytometry plots depicting the gating strategy to sort endothelial (CD31$^+$) and stromal (SCA-1$^+$CD51$^+$) enriched fractions from BM and collagenased bone of murine fetuses (E17) for scRNA-seq.

(legend continued on next page)

score [NES], 4.06; false discovery rate [FDR] q < 0.0001) and GO pathway analysis relating the transcriptome to extracellular matrix formation and skeletal development (Figure S5D).

Vice versa, separate re-clustering of all cells expressing the stromal marker *Prxx1* (Figure S5A) identified the same subset of cells characterized by co-expression of endothelial transcripts, mesenchymal transcripts, and transcription factors involved in EndoMT regulation in the "stromal" *Prxx1*$^+$ population of cells (Figure S5B). This population was separated from other stromal clusters by endothelial gene expression, reduced expression of genes encoding stromal factors, and GO pathways signaling vascular morphogenesis and endothelial migration (Figures S5C and S5E).

Next, to further corroborate the notion that the EndoMT population is indeed derived from ECs and represents an intermediate differentiation stage toward BMSCs, we performed a trajectory analysis, which sorts ECs and BMSCs at distinct extremes of pseudotime space (Figure 4G). Interestingly, EndoMT cells (cluster 4 in Figure 4D) were mostly enriched in the branch localized between ECs and BMSCs (Figures 4H and 4I), with a stepwise increase in expression of EndoMT markers during pseudotime (Figure 4G, inset), supporting the notion that some ECs may progressively acquire a stromal identity.

The scRNA-seq data confirm the presence of cells in nascent murine BM that express transcripts of endothelial and stromal lineages, in concert with transcription factors driving EndoMT, other EndoMT factors, and *Cxcl12*, which is in line with our human data and consistent with the view that these cells may represent ECs undergoing transdifferentiation toward stromal cell fates, as supported by scRNA-seq cell fate analysis.

eBMSCs contribute to BM tissue and niche formation in mice

To provide a formal experimental definition of EndoMT contributing to hematopoietic BM niche formation, lineage tracing experiments were performed using *VE-cadherin-Cre*;*LoxP-tdTomato* mice (Chen et al., 2009; Madisen et al., 2010). In these mice, CD144$^+$ ECs and their downstream developmental progeny are marked permanently by tdTomato fluorescence. In line with previous reports establishing the concept of EHT (endothelial-to-hematopoietic transition) (Boisset et al., 2010; Chen et al., 2009), the majority of CD45$^+$ hematopoietic cells as well as CD31$^+$CD144$^+$ ECs in 3-week-old mice expressed the tdTomato reporter (Figures S6A and S6B). Strikingly, a significant proportion (49.7% ± 1.6%) of highly purified BM stromal cells, defined by CD45$^-$Ter119$^-$CD31$^-$CD144$^-$Sca1$^+$CD51$^+$(Pdgfrα^+) marker expression and known to contain SSCs (Morikawa et al., 2009b; Pinho et al., 2013; Schepers et al., 2012), was found to be of endothelial origin, as indicated by tdTomato expression (Figures 5A and 5B). In addition, a substantial subset (25.8% ± 2.5%) of downstream osteo/chondrolineage (progenitor) cells (OLCs; CD45$^-$TER119$^-$CD31$^-$CD144$^-$Sca1$^-$CD51$^+$ cells; Lundberg et al., 2007; Schepers et al., 2012) was also derived from ECs (Figures 5A and 5B). *VE-cadherin-Cre*-negative;-*LoxP-tdTomato* mice were used as a negative control to determine the positive tdTomato fluorescence signal (Figure 5A, bottom panels). Immunofluorescence of the BM of *VE-cadherin-Cre*;*LoxP-tdTomato* mice confirmed the presence of tdTomato$^+$ bone-lining cells and osteolineage cells (osteocytes) (Figure S6A).

The contribution of endothelium-derived elements to the stromal BM compartment was sustained over time with 28.5% (±6.3) of BMSCs and 41.1% (±0.5) of OLCs being tdTomato positive in 11-week-old mice (Figure 5B).

TdTomato$^+$ BMSCs displayed considerably lower levels of tdTomato expression in comparison with ECs and hematopoietic cells (Figures S6A and S6B), likely explaining the absence of stromal elements in VE-cadherin reporter models when isolating only the tdTomato^{2+} population (Tikhonova et al., 2019). In addition, the increased sensitivity and recombination efficacy of the VE-cadherin reporting strain (https://www.jax.org/strain/017968) may contribute to identification of a subset of stromal cells originating from ECs in our studies.

Massive parallel RNA-seq of endothelium-derived (tdTomato-positive) versus non-endothelium-derived (tdTomato-negative) BMSC and OLC subsets confirmed the stromal nature of both subsets (high expression of stromal markers with absence of *Cdh5* expression) (Figure S6C). The endothelial origin of a subset of BM stromal cells was further confirmed by a robust contribution of tdTomato-positive cells to non-endothelial stromal cultures, established from whole BM or bone chips of 3- and 11-week-old *VE-cadherin-Cre*;*LoxP-tdTomato* mice (Figures S6H and S6I).

Endothelium-derived stromal cells isolated directly from murine BM were strikingly distinct transcriptionally, as defined by hierarchical clustering (Figure 5C). Differential gene expression included markedly higher expression of genes encoding key HSC regulatory factors (including *Cxcl12*, *Angpt1*, and *Kitl*) (Figures 5D and 5E) and *Lepr*, a gene used to define CXCL12-expressing HSC niche cells (Zhou et al., 2014; Figure 5E), as well as gene set enrichment indicative of cytokine regulation (Figure S6D). Endothelium-derived OLCs also overexpressed genes

(B) Uniform manifold approximation and projection (UMAP) plot showing unbiased clustering of endothelial (*Cdh5*, *Pecam1*, and *Eng*) and stromal clusters (*Col1a1*, *Prrx1*, and *Ngfr*).

(C–F) Clustering of ECs based on expression of the endothelial marker *Cdh5* (normalized expression level > 0; C) reveals a population (cluster 4) with transcriptional wiring indicative of ECs undergoing EndoMT, including co-expression of endothelial (*Cdh5*, *Pecam1*, and *Eng*), stromal (*Col1a1* and *Prrx1*), and known EndoMT driver genes (*Twist1*, *Snai2*, and *Zeb2*), activation of a mesenchymal transition program (D), and expression of *Nfgr* (E). Also shown are (F) Violin plots showing the relative reduction in expression of endothelial genes with concomitant increased expression of stromal transcripts, EndoMT-associated genes (*Cspg4* and *Fap*), mesenchymal transition drivers, and the hematopoietic factor *Cxcl12* in cluster 4 in comparison with other endothelial clusters. *adj. p value < 0.001.

(G) Lineage trajectory analysis demonstrating lineage relationship between ECs and BMSCs. Pseudotime analysis sorts ECs in left branches (1, 2, 3, and 4) and BMSCs in the right branches (6 and 7). Inset: increasing expression of the BMSC markers *Col1a1* and *Twist1* in branches 5, 6, and 7.

(H and I) Cells of cluster 4 (D), highlighted in red, are mostly located between ECs and BMSCs (H) with significant enrichment in branches 4, 5, and 6 by Fisher's exact test (I). ***p < 0.0001, *p-adj < 0.05.

See also Figure S5.

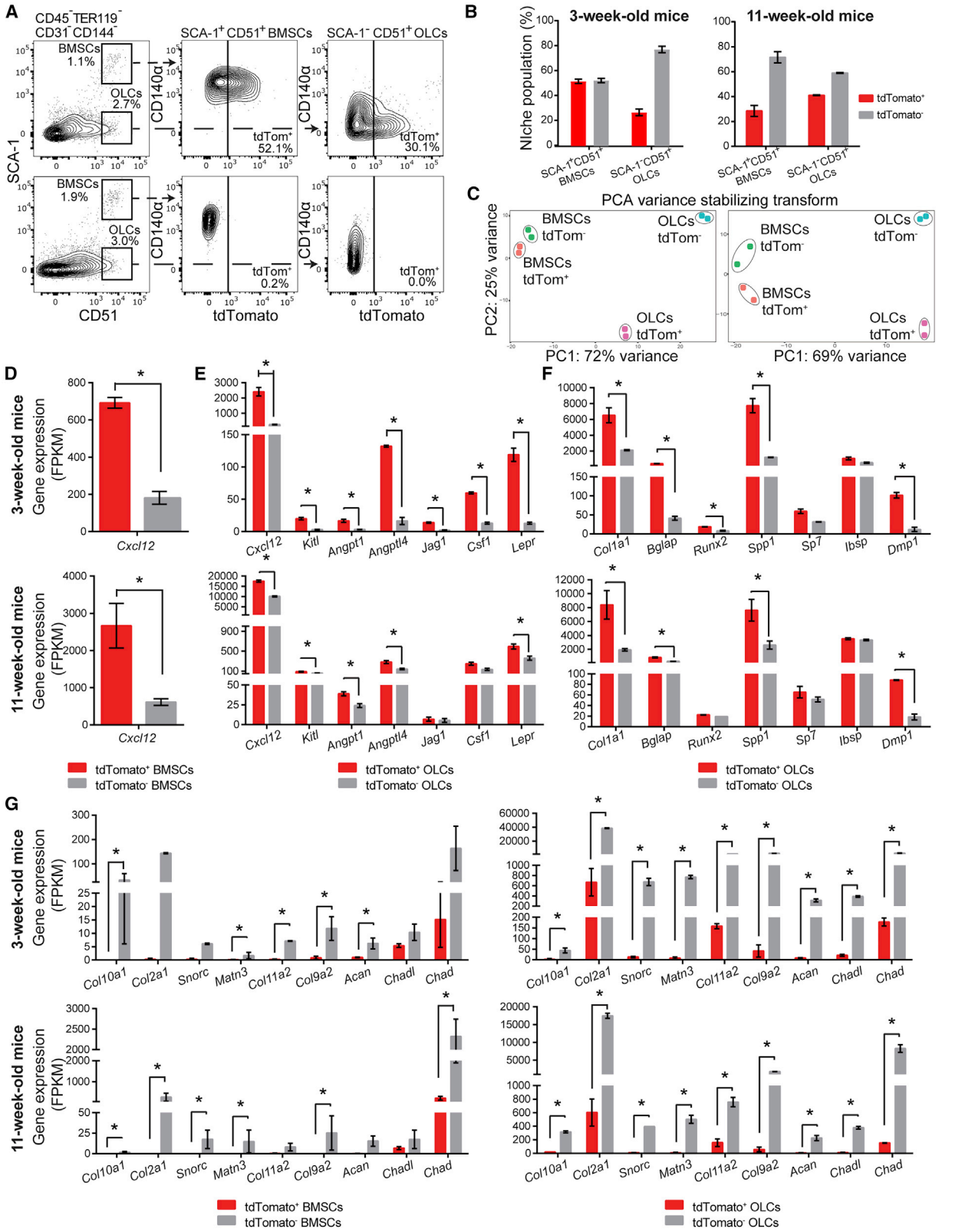

Figure 5. eBMSCs contribute to hematopoietic niche formation in mice

(A) Representative flow cytometry plots depicting the gating strategy to identify multipotent stromal cells (BMSCs) and osteo/chondrolineage progenitor cells (OLCs) in 3-week-old *VE-cadherin-Cre*;*LoxP-tdTomato* mice. A substantial subset of these stromal populations is derived from ECs, as indicated by tdTomato

(legend continued on next page)

typically associated with osteogenesis and osteoblast maturation (Figure 5F). Non-endothelium-derived stromal cells, in contrast, displayed striking differential expression of genes associated with chondrogenesis, including those encoding substituents of the collagenous extracellular matrix, such as *Acan*, *Col9a2*, and *Col11a2* (Figure 5G), reflected in enrichment of gene signatures indicative of chondrogenic matrix formation (Figures S6E and S6G).

These data reveal the existence of a distinct osteogenic subset of stromal cells in the murine BM that is of endothelial origin and differentially expresses key HSC regulatory factors, in line with the notion that these cells contribute to bone and hematopoietic niche formation. The data corroborate our findings in humans demonstrating the potential of LNGR$^+$ eBMSCs to form bone and BM tissue supporting hematopoiesis.

IL-33 is expressed in endothelial subsets during development and drives conversion of human fetal ECs to osteolineage cells via EndoMT

The lineage tracing experiments in mice establish that ECs give rise to BM stromal niche cells in development, suggesting EndoMT as a novel avenue of BMSC generation. Building on this notion, we sought to demonstrate that human LNGFR$^-$ ECs can give rise to LNGFR$^+$ ECs with stromal characteristics and interrogate the underlying mechanisms that drive EndoMT in human BM. Previously, we identified IL-33 as an anabolic factor in human hematopoiesis, angiogenesis, and osteogenesis, driving BM regeneration and development (Kenswil et al., 2018). IL-33 protein is increased in small subsets of ECs during development and regeneration, in comparison with steady-state postnatal ECs (Kenswil et al., 2018), together with factors such as BMP4 and DPP-4, known drivers of EndoMT. In human fetal BM, *IL33* was differentially expressed in LNGFR$^+$ hRECs and LNGFR$^-$ hRECs (Figure 6A). In E17 mouse BM, *Il33* expression was detected specifically in the EndoMT cluster of *Cdh5*-expressing ECs as well as in stromal subsets (Figures S5F and S5G).

Because IL-33 is an inflammatory cytokine, and inflammation is a known driving force of EndoMT, we tested whether IL-33 drives EndoMT in venous endothelium of fetal origin. To this end, we exposed human umbilical vein ECs (HUVECs) to increasing concentrations of IL-33 and compared the effects with TGF-β1, arguably the best-documented and most potent driver of EndoMT currently known (van Meeteren and ten Dijke, 2012; Zeisberg et al., 2007). EndoMT is associated with transcriptional alterations in ECs (Kovacic et al., 2019; Piera-Velazquez and Jimenez, 2019), primarily induced by the transcriptional regulators *SNAI1* (Snail family transcriptional repressor 1), *SNAI2* (Snail family transcriptional repressor 2 or *SLUG*), and *TWIST1* (Souilhol et al., 2018). Exposure of HUVECs to IL-33 led to increased expression of *SNAI2* and *TWIST1* but not *SNAI1* (Figure 6B), strikingly recapitulating overexpression of these specific transcription factors in primary human LNGFR$^+$ hRECs (Figure 2F).

Concurrent with the increased expression of *SNAI2*, which is a zinc-finger transcriptional repressor that can bind to the E-box of promoters of endothelial lineage genes (Nieto, 2002), expression of the endothelial markers CD31, CD34, and CD144 was decreased in a dose-dependent manner (Figure 6D). Loss of EC identity was corroborated by decreased gene expression of *CDH5*, *PECAM1*, *TEK*, *VEGFR2*, and *vWF* by IL-33 (Figure 6C and data not shown).

EndoMT, like EMT, is not only characterized by loss of endothelial markers but also attenuation of EC functional integrity and apical-basal polarity to acquire stromal behavior in a transitional process driven by the aforementioned transcription factors (Yang et al., 2020). Using electric cell-substrate impedance sensing (ECIS), we monitored endothelial barrier function in HUVECs in response to exogenous IL-33 (Adams et al., 2013; Halaidych et al., 2018; Patsch et al., 2015). Treatment with IL-33 disrupted the functional barrier integrity and cell-matrix interactions of HUVECs (Figures 6E–6G), suggesting that IL-33 triggers a transcriptional program in ECs that eventually compromises endothelial identity.

Concurrent with the increased expression of *TWIST1*, which is a basic helix-loop-helix transcriptional activator of stromal gene expression (Wang et al., 1997), IL-33 induced expression of stromal markers (LNGFR/CD271 and CD44) in a dose-dependent manner (Figure 6D). This was corroborated by demonstrating increased expression of other *bona fide* stromal markers such as *FAP*, *TAGLN* (transgelin encoding SM22-α), and *ACTA2* (actin alpha 2 encoding alpha-smooth muscle actin [α-SMA]) (Figures 6C and 6I). Remarkably, IL-33 induced these EndoMT-defining transcriptional programs in HUVECs as a single agent to an extent similar to TGF-β1, arguably the most potent inducer of EndoMT currently known (Figure 6D).

Next, to investigate whether HUVECs not only acquired immunophenotypic changes indicative of EndoMT but also cellular properties congruent with transition from an endothelial identity toward stromal cell fates, we performed assays interrogating the capacity of IL-33 to convert ECs into osteo-lineage cells with matrix deposition capacity. IL-33 induced expression of extracellular matrix molecules such as *FN*, *COL1A1*, and *COL3A1* (Figures 6H and 6I), and IL-33-exposed cells were capable of forming (calcified) matrix, as indicated by dose-dependent induction of alizarin red binding (Figure 6J), von Kossa staining to levels similar to *bona fide* BMSCs (Figure 6K), and alkaline phosphatase activity (Figure 6L).

expression (top panels). *VE-cadherin-Cre*-negative;*LoxP-tdTomato* mice (bottom panels) were used as a negative control to determine the positive tdTomato fluorescence signal.

(B) Frequency of tdTomato$^+$ cells within the BMSC and OLC populations of 3- and 11-week-old *VE-cadherin-Cre*;*LoxP-tdTomato* mice. n = 7 for 3-week-old mice, and n = 3 for 11-week-old mice.

(C) PCA of the transcriptomes of tdTomato$^+$ compared with tdTomato$^-$ BMSCs and OLCs showing distinct hierarchical clustering of cell populations in 3-week-old (n = 2) and 11-week-old mice (n = 2).

(D and E) Expression of genes encoding key HSC niche-associated factors in tdTomato$^+$ versus tdTomato$^-$ BMSCs (D) and OLCs (E).

(F and G) TdTomato$^+$ OLCs display overexpression of genes encoding transcripts related to osteogenesis (F), whereas tdTomato$^-$ BMSCs (left panels) and tdTomato$^-$ OLCs (right panels) overexpress transcripts related to chondrogenesis (G). *FDR < 0.05.

See also Figure S6.

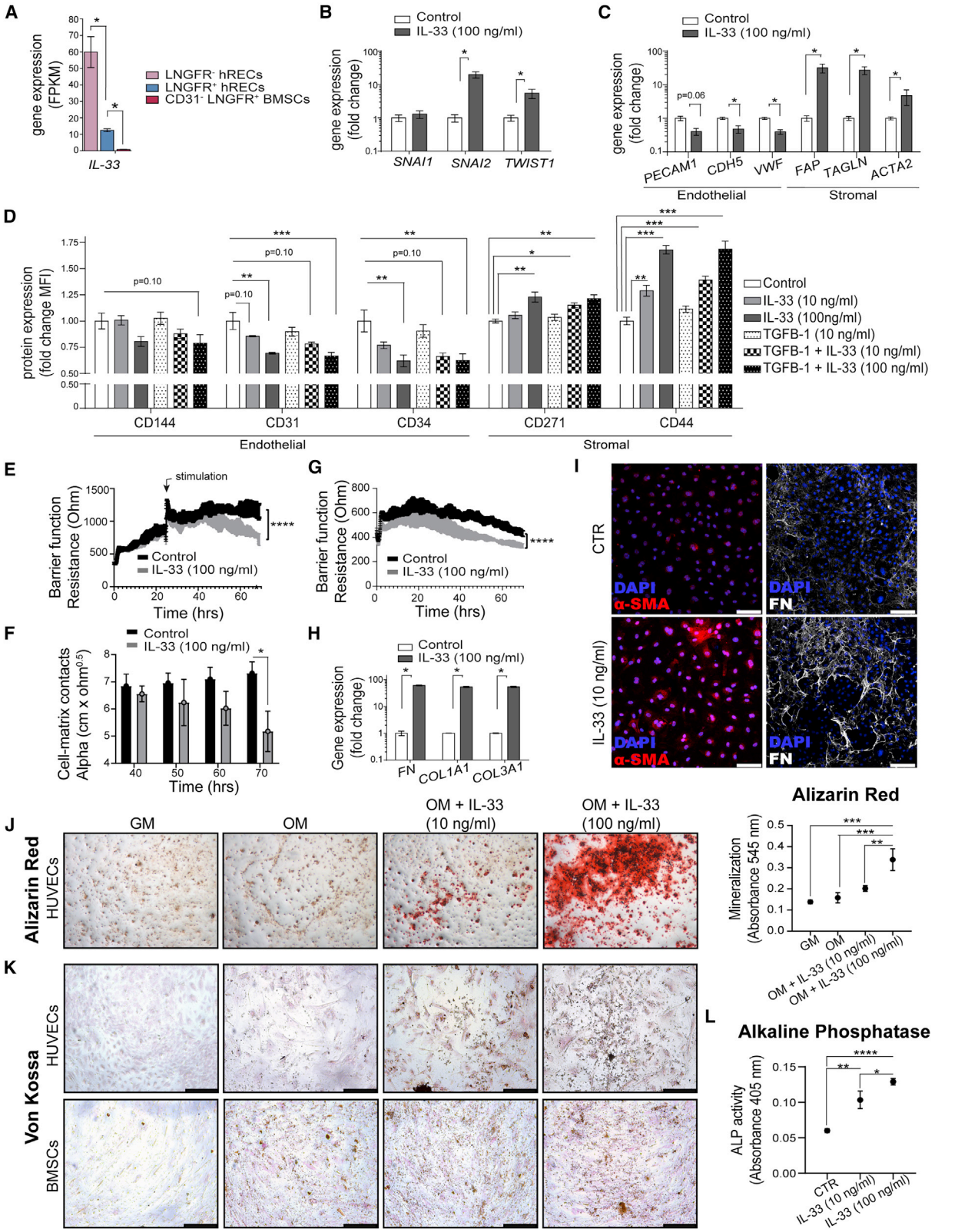

(legend on next page)

These data demonstrate that IL-33 is capable of inducing alterations in HUVECs indicative of cells undergoing EndoMT (Dejana et al., 2017), recapitulating characteristics of LNGFR$^+$ ECs identified in human BM (Figure 2), and converting fetal venous ECs to functional osteolineage cells with matrix deposition activity. Chondrogenic pellets could not be established from IL-33-exposed HUVECs, precluding *in vivo* transplantation of these cells, suggesting that transient IL-33 exposure is not enough to durably convert ECs to multipotent stromal cells with niche formation capacity.

IL-33 induces EndoMT in adult human ECs through ST2-SNAI2 signaling

Although HUVECs are widely used as an *in vitro* model to study EC biology, findings in this venous endothelium of fetal origin may not be applicable to ECs of adult origin, which may have reduced plasticity. To address this, we tested whether IL-33 can also induce EndoMT in endothelial colony-forming cells (ECFCs) isolated from adult peripheral blood, which have high proliferative potential and are able to contribute to vessel formation *in vivo* (Critser and Yoder, 2010). IL-33 (10 ng/mL and 100 ng/mL) induced a dose-dependent decrease in endothelial CD144 expression with a concomitant increase in the stromal markers α-SMA (encoded by *ACTA2*) (Figure S7A), faithfully recapitulating findings in HUVECs (Figures 6C, 6D, 6H, and 6I).

Similar to findings in HUVECs, exposure to IL-33 induced a permissive state for subsequent osteogenic differentiation of ECs, as indicated by dose-related generation of cells expressing early and late osteogenic differentiation markers (*COL1A1*, *RUNX2*, *OSX, DMP1, SOST*, and *BGLAP*) (Figures S7B and S7C) and matrix deposition capacity, as demonstrated by induction of alizarin red binding (Figure S7D), von Kossa staining (Figure S7E), and alkaline phosphatase activity (Figure S7F).

Finally, we sought to begin unraveling the underlying molecular mechanisms of IL-33-mediated EndoMT in human ECs. IL-33 is thought to function by binding to its cognate receptor ST2 (Kakkar and Lee, 2008). Blocking ST2 signaling in ECFCs by using a neutralizing antibody directed against ST2 (Guo et al., 2014; Suzukawa et al., 2008) resulted in partial rescue of IL-33-mediated EndoMT, as shown by reduced downregulation of CD144 and reduced upregulation of fibronectin, in particular at an IL-33 dose of 100 ng/mL (Figure S7G). Concomitantly, upregulation of *SNAI2* was impaired by the ST2-neutralizing antibody (Figure S7H).

These data demonstrate that LNGFR$^+$ "mesenchyme-primed" ECs, as identified in human development and regeneration, can be derived from fetal and adult human ECs by IL-33, expressed in endothelial subsets during development and regeneration, identifying IL-33 as a novel and strong inducer of EndoMT and conversion to osteogenic cell fates, at least partially, through ST2-SNAI2 signaling.

DISCUSSION

Stromal cells in the mammalian BM play pivotal roles in tissue maintenance and regeneration. They are likely heterogeneous, with subsets contributing to skeletogenesis, chondrogenesis, or support of hematopoiesis by providing niches to HSPCs. However, the developmental origins of such cells had remained incompletely understood.

Here we report prospective isolation of a mammalian EC-derived precursor that has the potential of *de novo* formation of BMSCs that establish the hematopoietic niche. LNGFR$^+$ ECs constitute a rare subset of ECs in homeostasis but are more prevalent during fetal development and re-emerge postnatally in the context of regeneration after injury. LNGFR$^+$ ECs can arise from IL-33 driven conversion of LNGFR$^-$ ECs and display transcriptional re-wiring consistent with stemness and EndoMT,

Figure 6. IL-33 drives EndoMT in human fetal ECs

(A) Expression of IL-33 in different niche subsets in human fetal BM. *FDR < 0.05.

(B and C) Expression of genes implicated in EndoMT in HUVECs treated with IL-33 for four consecutive days (n = 4) in comparison with the vehicle control (n = 4). *p < 0.05, Mann-Whitney *U* test.

(B) Upregulation of transcription factors driving EndoMT.

(C) Downregulation of genes encoding endothelial markers and upregulation of stromal genes.

(D) Protein expression of endothelial and stromal markers by HUVECs after treatment with IL-33, TGF-β1, or a combination (n = 3). One-way ANOVA was used to compare the fold change of the median fluorescence intensity (MFI) of each marker, followed by Dunnett's multiple comparisons test using vehicle control-treated HUVECs as the reference group. *p < 0.05, **p < 0.01, ***p < 0.001.

(E–G) Loss of endothelial functional properties upon IL-33 exposure.

(E) Endothelial barrier function during IL-33 stimulation (n = 4). ****p < 0.0001, unpaired t test. Mean ± SD.

(F) Bar graphs representing the integrity and strength of cell-matrix interactions (alpha) mathematically modeled from the impedance data in (E). **p < 0.01, multiple t test. Mean ± SD.

(G) Endothelial barrier function after pre-stimulation with IL-33. Mean ± SD. ****p < 0.0001, unpaired t test. Mean ± SD.

(H and I) Gain of stromal, matrix-depositing, functional properties upon IL-33 exposure.

(H) Upregulation of genes encoding extracellular matrix components in HUVECs treated with IL-33 for 4 days (n = 4). *p < 0.05, Mann-Whitney *U* test.

(I) Immunofluorescence labeling in HUVECs stimulated for 24 h with IL-33. α-SMA, alpha-smooth muscle actin; FN, fibronectin. 4′,6-Diamidino-2-phenylindole (DAPI) staining was used to visualize cell nuclei (representative data from n = 3). Scale bar, 100 μm.

(J–L) IL-33 converts HUVECs into osteolineage cells with matrix deposition capacity, as demonstrated by alizarin red staining (J) to visualize mineralized deposits in HUVECs cultured in regular growth medium (GM) or osteogenic medium (OM). A representative picture is shown. Right: quantification upon solubilization of mineral deposits with cetylpyridinium (n = 3). **p < 0.01, ***p < 0.001, one-way ANOVA followed by Tukey's multiple comparison test. Mean ± SD.

(K) Calcium deposits as demonstrated by von Kossa staining (representative data from n = 3). Scale bar, 250 μm.

(L) Alkaline phosphatase enzymatic assay. *p < 0.05, **p < 0.01, ***p < 0.001, one-way ANOVA followed by Tukey's multiple comparisons test. Mean ± SD. Each "n" represents a different HUVEC donor and independent experiment.

See also Figure S7.

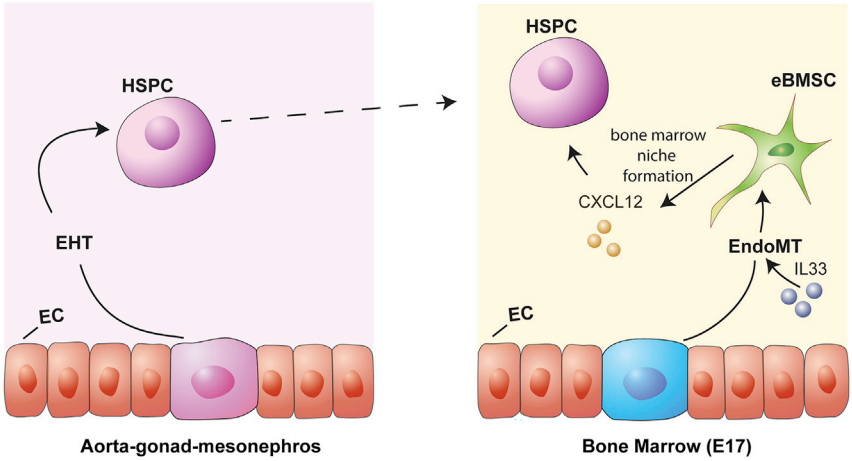

Figure 7. A model of EC contributions to development of the hematopoietic system in mammals

ECs contribute directly to hematopoiesis by giving rise to hematopoietic stem/progenitor cells (HSPCs) via endothelial-hematopoietic transition (EHT). In addition, ECs generate BMSCs that establish the hematopoietic niche via EndoMT with interleukin-33 (IL-33) as a candidate factor driving this process.

culminating in their ability to generate *bona fide* BMSCs with *in vivo* hematopoietic niche formation capacity. Formal experimental support for the notion that ECs can transition to distinct stromal cells with HSPC-supportive characteristics *in vivo* is provided by scRNA-seq and lineage tracing studies in mice. The data argue for an adapted conceptual view on the origins of the hematopoietic system in mammals, in which ECs not only generate HSCs (through the process of EHT; Boisset et al., 2010; Chen et al., 2009) but also distinct eBMSCs with BM niche generation capacity (Figure 7).

The possibility of the *de novo* generation of stromal cells through an EC intermediate has been suggested previously by cell culture experiments using embryonic stem cells (ESCs) and induced pluripotent stem cells (iPSCs), demonstrating that these stromal cell may be generated from mesenchymo-angioblasts via an endothelial-stage intermediate (Kumar et al., 2017; Vodyanik et al., 2010). *In vivo* precedence for the ability of ECs to transition to stromal cell fates has been provided by lineage tracing studies in mice, demonstrating that endocardial ECs are progenitors of pericytes and vascular smooth muscle cells in the murine embryonic heart (Chen et al., 2016a). These EC-derived stromal progenitors lacked the capacity to differentiate into osteogenic or adipogenic cells, suggesting that the skeletogenic differentiation capacity of EC-derived stromal progenitors may be tissue-restricted.

Whether the pool size of niche-generating eBMSCs is developmentally restricted or can be modulated by *de novo* generation of eBMSCs through EndoMT in times of "tissue demand" remains unknown. Our identification of ECs with EndoMT characteristics in humans after BM injury suggests the latter possibility. Future investigations, including conditional lineage tracing experiments in mice, will likely answer this question, perhaps opening the way to pharmacologic harnessing of EndoMT to foster BM regeneration.

In this context, it is relevant that we identify IL-33 as a potent driver of EndoMT with likely relevance to human physiology. Transcriptional profiling of EC subsets emerging during regeneration earlier identified IL-33 as an anabolic factor stimulating hematopoiesis and osteogenesis (Kenswil et al., 2018). Remarkably, IL-33 was able to induce EndoMT in HUVECs as a single agent to an extent similar to TGF-β1, arguably the most potent inducer of EndoMT currently known. Mechanistically, exposure to IL-33 resulted in simultaneous upregulation of *SNAI2* and *TWIST1*, important transcriptional regulators of EndoMT through Hedgehog signaling, in line with the molecular profile of LNGFR$^+$ ECs isolated from the human marrow. Inhibition of the canonical IL-33 receptor ST2 attenuated *SNAI2* upregulation and induction of an EndoMT phenotype, although the signaling underlying IL-33-mediated EndoMT remains largely to be elucidated, and other receptors may be involved. These observations warrant further research of the effect of this inflammation-associated cytokine in cellular reprogramming, including acquisition of stemness features.

The data reveal a previously unappreciated potential of BM ECs to convert to niche-generating eBMSCs. Elucidation of this process and its associated molecular programs is anticipated to foster investigations into its relevance for development, regeneration, and disease.

Limitations of study

The combined human and murine experimental data, including cellular and transcriptional characterization of endothelial subsets, genetic lineage tracing, single-cell trajectory analyses, and *ex vivo* mechanistic studies, are congruent with the view that ECs transition toward tissue-generating BMSCs that contribute to BM formation. Whether ECs transition into *bona fide* stromal stem cells with multi-lineage tissue differentiation or generate a more heterogeneous population of stromal stem/progenitor cells with distinct, restricted differentiation capacities that, in a composite manner, contribute to BM formation remains to be fully elucidated and will require further studies at clonal resolution. IL-33 is expressed in EC and stromal subsets in the developing and regenerating BM and is identified as a novel driver of EndoMT by extensive *in vitro* experimentation, demonstrating its ability to convert ECs into stromal cells. The *in vivo* contributions of IL-33 to the EndoMT occurring in development and, possibly, in regeneration, however, remain to be fully established and its relative contribution to be elucidated. Redundancy may be anticipated because other factors known to drive EndoMT, such as BMP4 and DPP-4, are expressed in human endothelial subsets during development. In this context, it may be of substantial interest and instructive to extend investigations of IL-33-mediated EndoMT to pathological processes because IL-33 is overexpressed in human fibrotic conditions characterized by expansion of stromal cells and pathological deposition of extracellular matrices,

including myelofibrosis, liver fibrosis, and lung fibrosis (Kotsiou et al., 2018).

STAR★METHODS

Detailed methods are provided in the online version of this paper and include the following:

- KEY RESOURCES TABLE
- RESOURCE AVAILABILITY
  - Lead contact
  - Materials availability
  - Data and code availability
- EXPERIMENTAL MODEL AND SUBJECT DETAILS
  - Animal models
  - Human subjects
  - Primary cultures
- METHOD DETAILS
  - Human bone (marrow) cell isolation
  - Fluorescence-activated cell sorting (FACS) of human niche cells
  - Immunocytochemistry to detect CD31, CD105, and CD271 on human niche cells
  - Multiplex immunofluorescence staining to detect CD31, CD105 and CD271 in fetal bone
  - Bulk-RNA Sequencing and gene set enrichment analysis (GSEA)
  - Human stromal cell flow cytometry analysis
  - Fibroblast colony-forming efficiency assay
  - Co-culture of hematopoietic stem/progenitor cells with the stromal progeny of LNGFR^{+} ECs and CD31^{-}LNGFR^{+} BMSCs
  - Quantification and multiparametric immunophenotyping of cultured HSPCs
  - Human hematopoietic colony forming-unit assay
  - Subcutaneous implantation of chondrogenically primed pellets containing LNGFR^{+} ECs-derived stromal cells
  - Histological analysis and immunohistochemistry of 3D pellets
  - Immunohistochemistry for human glyceraldehyde-3-phosphate dehydrogenase (hGAPDH)
  - Immunohistochemistry for mouse CD45 (mCD45)
  - Isolation and ScRNaseq of stromal cells and ECs from murine fetal bone
  - Single cell library construction and sequencing
  - Single cell RNA sequencing data analysis
  - Pseudotime analysis
  - FACS of murine niche cells
  - Immunofluorescence imaging of murine sternum
  - Murine stromal cell flow cytometry analysis
  - ECFC and HUVEC RNA extraction and gene expression analyses
  - HUVEC flow cytometry analyses
  - HUVEC endothelial barrier function assays
  - Immunofluorescent labeling of endothelial cells
  - Osteogenic, adipogenic, and chondrogenic differentiation assays
  - Osteogenic differentiation assays in endothelial cells
- QUANTIFICATION AND STATISTICAL ANALYSIS

SUPPLEMENTAL INFORMATION

Supplemental information can be found online at https://doi.org/10.1016/j.stem.2021.01.006.

ACKNOWLEDGMENTS

We would like to thank Dr. Kirsten van Lom, Dr. Eric Braakman, Lucia Duinhouwer, and Mariëtte ter Borg for providing CD34^{+} cells and help with human BM sampling; Natalie Papazian for helping to process fetal tissue; Dr. Elwin Rombouts, Peter van Geel, and Michael Vermeulen for operating the BD FACSARIA III; Maria Mylona, Maria Adisty, and Paulette van Strien for performing FACs and RNA-seq; Onno Roovers, Almira Henić, Eline Pronk, Gert-Jan Kremers, Bella Banjanin, Ursula Stalmann, Nils Bayer, and Madelon de Jong for providing technical advice and assistance; Esther Siteur-van Rijnstra and Cynthia van der Linden for providing technical assistance with fetal tissue; Mathias Francois and lab members for help with the lineage tracing experiments; Emma de Pater for advice concerning mouse breeding; members of the Erasmus MC Department of Hematology for scientific discussions; and Egied Simons for assisting with illustrations. This work was supported by an Erasmus MC fellowship award (to M.H.G.P.R.). M.-J.G. and G.S.-D. are supported by the Netherlands CardioVascular Research Initiative: the Dutch Heart Foundation, Dutch Federation of University Medical Centers, Netherlands Organization for Health Research and Development, and the Royal Netherlands Academy of Sciences (grant CVON 2014-11 RECONNECT). G.S.-D. is also sponsored by a trampoline grant (#22379) from AFM-Telethon and FOP Italia (Grant Italia 2020). A.L. is supported by the European Union Horizon 2020 Research and Innovation Program under grant agreement 801159.

AUTHOR CONTRIBUTIONS

K.J.G.K., P.P., and G.S.-D. designed and performed experiments, analyzed and visualized the data, and wrote the manuscript. C.v.D. and A.L. designed and performed experiments and analyzed and visualized data. K.L. performed experiments and analyzed and visualized data. C.K., B.V., A.C.J., J.F., and E.M.J.B. provided input on and performed experiments and analyzed data. R.M.H. and M.A.S. performed the bioinformatics analyses for the RNA-seq data. I.G.C. and R.L. performed and described scRNA-seq analyses. B.B. provided human fetal samples. P.K.B. provided human hip bone samples and input on experiments. M.-J.G. and P.t.D. provided ECFCs and input on experiments. T.C. provided human fetal samples and input on experiments. E.F. provided BMSCs and input on experiments. G.K. provided HUVECs and input on experiments and analyzed data. M.H.G.P.R. conceived the program, designed the experiments, analyzed the data, wrote the manuscript, supervised the study, and acquired funding.

DECLARATION OF INTERESTS

The authors declare no competing interests.

Received: March 20, 2020
Revised: September 29, 2020
Accepted: January 11, 2021
Published: February 8, 2021

REFERENCES

Adams, W.J., Zhang, Y., Cloutier, J., Kuchimanchi, P., Newton, G., Sehrawat, S., Aird, W.C., Mayadas, T.N., Luscinskas, F.W., and García-Cardeña, G. (2013). Functional vascular endothelium derived from human induced pluripotent stem cells. Stem Cell Reports *1*, 105–113.

Ansieau, S., Bastid, J., Doreau, A., Morel, A.P., Bouchet, B.P., Thomas, C., Fauvet, F., Puisieux, I., Doglioni, C., Piccinin, S., et al. (2008). Induction of EMT by twist proteins as a collateral effect of tumor-promoting inactivation of premature senescence. Cancer Cell *14*, 79–89.

Azhar, M., Runyan, R.B., Gard, C., Sanford, L.P., Miller, M.L., Andringa, A., Pawlowski, S., Rajan, S., and Doetschman, T. (2009). Ligand-specific function

of transforming growth factor beta in epithelial-mesenchymal transition in heart development. Dev. Dyn. *238*, 431–442.

Bianco, P., and Cossu, G. (1999). Uno, nessuno e centomila: searching for the identity of mesodermal progenitors. Exp. Cell Res. *251*, 257–263.

Bianco, P., Robey, P.G., and Simmons, P.J. (2008). Mesenchymal stem cells: revisiting history, concepts, and assays. Cell Stem Cell *2*, 313–319.

Boisset, J.C., van Cappellen, W., Andrieu-Soler, C., Galjart, N., Dzierzak, E., and Robin, C. (2010). In vivo imaging of haematopoietic cells emerging from the mouse aortic endothelium. Nature *464*, 116–120.

Bracken, C.P., Gregory, P.A., Kolesnikoff, N., Bert, A.G., Wang, J., Shannon, M.F., and Goodall, G.J. (2008). A double-negative feedback loop between ZEB1-SIP1 and the microRNA-200 family regulates epithelial-mesenchymal transition. Cancer Res. *68*, 7846–7854.

Brown, C., McKee, C., Bakshi, S., Walker, K., Hakman, E., Halassy, S., Svinarich, D., Dodds, R., Govind, C.K., and Chaudhry, G.R. (2019). Mesenchymal stem cells: Cell therapy and regeneration potential. J. Tissue Eng. Regen. Med. *13*, 1738–1755.

Chakraborty, S., Wirrig, E.E., Hinton, R.B., Merrill, W.H., Spicer, D.B., and Yutzey, K.E. (2010). Twist1 promotes heart valve cell proliferation and extracellular matrix gene expression during development in vivo and is expressed in human diseased aortic valves. Dev. Biol. *347*, 167–179.

Chan, C.K.F., Seo, E.Y., Chen, J.Y., Lo, D., McArdle, A., Sinha, R., Tevlin, R., Seita, J., Vincent-Tompkins, J., Wearda, T., et al. (2015). Identification and specification of the mouse skeletal stem cell. Cell *160*, 285–298.

Chen, M.J., Yokomizo, T., Zeigler, B.M., Dzierzak, E., and Speck, N.A. (2009). Runx1 is required for the endothelial to haematopoietic cell transition but not thereafter. Nature *457*, 887–891.

Chen, Q., Zhang, H., Liu, Y., Adams, S., Eilken, H., Stehling, M., Corada, M., Dejana, E., Zhou, B., and Adams, R.H. (2016a). Endothelial cells are progenitors of cardiac pericytes and vascular smooth muscle cells. Nat. Commun. *7*, 12422.

Chen, S., Zambetti, N.A., Bindels, E.M.J., Kenswill, K., Mylona, A.M., Adisty, N.M., Hoogenboezem, R.M., Sanders, M.A., Cremers, E.M.P., Westers, T.M., et al. (2016b). Massive parallel RNA sequencing of highly purified mesenchymal elements in low-risk MDS reveals tissue-context-dependent activation of inflammatory programs. Leukemia *30*, 1938–1942.

Coşkun, S., Chao, H., Vasavada, H., Heydari, K., Gonzales, N., Zhou, X., de Crombrugghe, B., and Hirschi, K.K. (2014). Development of the fetal bone marrow niche and regulation of HSC quiescence and homing ability by emerging osteolineage cells. Cell Rep. *9*, 581–590.

Cossu, G., and Bianco, P. (2003). Mesoangioblasts–vascular progenitors for extravascular mesodermal tissues. Curr. Opin. Genet. Dev. *13*, 537–542.

Crampton, S.P., Davis, J., and Hughes, C.C.W. (2007). Isolation of human umbilical vein endothelial cells (HUVEC). J. Vis. Exp. (3), 183.

Crisan, M., Yap, S., Casteilla, L., Chen, C.W., Corselli, M., Park, T.S., Andriolo, G., Sun, B., Zheng, B., Zhang, L., et al. (2008). A perivascular origin for mesenchymal stem cells in multiple human organs. Cell Stem Cell *3*, 301–313.

Critser, P.J., and Yoder, M.C. (2010). Endothelial colony-forming cell role in neoangiogenesis and tissue repair. Curr. Opin. Organ Transplant. *15*, 68–72.

Dejana, E., Hirschi, K.K., and Simons, M. (2017). The molecular basis of endothelial cell plasticity. Nat. Commun. *8*, 14361.

Dominici, M., Le Blanc, K., Mueller, I., Slaper-Cortenbach, I., Marini, F., Krause, D., Deans, R., Keating, A., Prockop, Dj., and Horwitz, E. (2006). Minimal criteria for defining multipotent mesenchymal stromal cells. The International Society for Cellular Therapy position statement. Cytotherapy *8*, 315–317.

Durinck, S., Spellman, P.T., Birney, E., and Huber, W. (2009). Mapping identifiers for the integration of genomic datasets with the R/Bioconductor package biomaRt. Nat. Protoc. *4*, 1184–1191.

Eisenberg, L.M., and Markwald, R.R. (1995). Molecular regulation of atrioventricular valvuloseptal morphogenesis. Circ. Res. *77*, 1–6.

Farrell, E., Both, S.K., Odörfer, K.I., Koevoet, W., Kops, N., O'Brien, F.J., Baatenburg de Jong, R.J., Verhaar, J.A., Cuijpers, V., Jansen, J., et al. (2011). In-vivo generation of bone via endochondral ossification by in-vitro chondrogenic priming of adult human and rat mesenchymal stem cells. BMC Musculoskelet. Disord. *12*, 31.

Greenbaum, A., Hsu, Y.M.S., Day, R.B., Schuettpelz, L.G., Christopher, M.J., Borgerding, J.N., Nagasawa, T., and Link, D.C. (2013). CXCL12 in early mesenchymal progenitors is required for haematopoietic stem-cell maintenance. Nature *495*, 227–230.

Guo, Z., Wu, J., Zhao, J., Liu, F., Chen, Y., Bi, L., Liu, S., and Dong, L. (2014). IL-33 promotes airway remodeling and is a marker of asthma disease severity. J. Asthma *51*, 863–869.

Halaidych, O.V., Freund, C., van den Hil, F., Salvatori, D.C.F., Riminucci, M., Mummery, C.L., and Orlova, V.V. (2018). Inflammatory Responses and Barrier Function of Endothelial Cells Derived from Human Induced Pluripotent Stem Cells. Stem Cell Reports *10*, 1642–1656.

Hurlstone, A.F.L., Haramis, A.P.G., Wienholds, E., Begthel, H., Korving, J., Van Eeden, F., Cuppen, E., Zivkovic, D., Plasterk, R.H.A., and Clevers, H. (2003). The Wnt/β-catenin pathway regulates cardiac valve formation. Nature *425*, 633–637.

Isern, J., García-García, A., Martín, A.M., Arranz, L., Martín-Pérez, D., Torroja, C., Sánchez-Cabo, F., and Méndez-Ferrer, S. (2014). The neural crest is a source of mesenchymal stem cells with specialized hematopoietic stem cell niche function. eLife *3*, e03696.

Jones, E., English, A., Churchman, S.M., Kouroupis, D., Boxall, S.A., Kinsey, S., Giannoudis, P.G., Emery, P., and McGonagle, D. (2010). Large-scale extraction and characterization of CD271+ multipotential stromal cells from trabecular bone in health and osteoarthritis: implications for bone regeneration strategies based on uncultured or minimally cultured multipotential stromal cells. Arthritis Rheum. *62*, 1944–1954.

Kakkar, R., and Lee, R.T. (2008). The IL-33/ST2 pathway: therapeutic target and novel biomarker. Nat. Rev. Drug Discov. *7*, 827–840.

Kenswil, K.J.G., Jaramillo, A.C., Ping, Z., Chen, S., Hoogenboezem, R.M., Mylona, M.A., Adisty, M.N., Bindels, E.M.J., Bos, P.K., Stoop, H., et al. (2018). Characterization of Endothelial Cells Associated with Hematopoietic Niche Formation in Humans Identifies IL-33 As an Anabolic Factor. Cell Rep. *22*, 666–678.

Kfoury, Y., and Scadden, D.T. (2015). Mesenchymal cell contributions to the stem cell niche. Cell Stem Cell *16*, 239–253.

Kokudo, T., Suzuki, Y., Yoshimatsu, Y., Yamazaki, T., Watabe, T., and Miyazono, K. (2008). Snail is required for TGFbeta-induced endothelial-mesenchymal transition of embryonic stem cell-derived endothelial cells. J. Cell Sci. *121*, 3317–3324.

Kotsiou, O.S., Gourgoulianis, K.I., and Zarogiannis, S.G. (2018). IL-33/ST2 axis in organ fibrosis. Front. Immunol. *9*, 2432.

Kovacic, J.C., Dimmeler, S., Harvey, R.P., Finkel, T., Aikawa, E., Krenning, G., and Baker, A.H. (2019). Endothelial to Mesenchymal Transition in Cardiovascular Disease: JACC State-of-the-Art Review. J. Am. Coll. Cardiol. *73*, 190–209.

Kumar, A., D'Souza, S.S., Moskvin, O.V., Toh, H., Wang, B., Zhang, J., Swanson, S., Guo, L.W., Thomson, J.A., and Slukvin, I.I. (2017). Specification and Diversification of Pericytes and Smooth Muscle Cells from Mesenchymoangioblasts. Cell Rep. *19*, 1902–1916.

Kusumbe, A.P., Ramasamy, S.K., and Adams, R.H. (2014). Coupling of angiogenesis and osteogenesis by a specific vessel subtype in bone. Nature *507*, 323–328.

Kusumbe, A.P., Ramasamy, S.K., Itkin, T., Mäe, M.A., Langen, U.H., Betsholtz, C., Lapidot, T., and Adams, R.H. (2016). Age-dependent modulation of vascular niches for haematopoietic stem cells. Nature *532*, 380–384.

Lee, H.T., Lee, J.G., Na, M., and Kay, E.P. (2004). FGF-2 induced by interleukin-1 β through the action of phosphatidylinositol 3-kinase mediates endothelial mesenchymal transformation in corneal endothelial cells. J. Biol. Chem. *279*, 32325–32332.

Lerner, C., and Harrison, D.E. (1990). 5-Fluorouracil spares hemopoietic stem cells responsible for long-term repopulation. Exp. Hematol. *18*, 114–118.

Li, H., Ghazanfari, R., Zacharaki, D., Ditzel, N., Isern, J., Ekblom, M., Méndez-Ferrer, S., Kassem, M., and Scheding, S. (2014). Low/negative expression of

PDGFR-α identifies the candidate primary mesenchymal stromal cells in adult human bone marrow. Stem Cell Reports *3*, 965–974.

Love, M.I., Huber, W., and Anders, S. (2014). Moderated estimation of fold change and dispersion for RNA-seq data with DESeq2. Genome Biol. *15*, 550.

Lundberg, P., Allison, S.J., Lee, N.J., Baldock, P.A., Brouard, N., Rost, S., Enriquez, R.F., Sainsbury, A., Lamghari, M., Simmons, P., et al. (2007). Greater bone formation of Y2 knockout mice is associated with increased osteoprogenitor numbers and altered Y1 receptor expression. J. Biol. Chem. *282*, 19082–19091.

Madisen, L., Zwingman, T.A., Sunkin, S.M., Oh, S.W., Zariwala, H.A., Gu, H., Ng, L.L., Palmiter, R.D., Hawrylycz, M.J., Jones, A.R., et al. (2010). A robust and high-throughput Cre reporting and characterization system for the whole mouse brain. Nat. Neurosci. *13*, 133–140.

Mahmoud, M.M., Serbanovic-Canic, J., Feng, S., Souilhol, C., Xing, R., Hsiao, S., Mammoto, A., Chen, J., Ariaans, M., Francis, S.E., et al. (2017). Shear stress induces endothelial-to-mesenchymal transition via the transcription factor Snail. Sci. Rep. *7*, 3375.

Markwald, R.R., Fitzharris, T.P., and Smith, W.N.A. (1975). Sturctural analysis of endocardial cytodifferentiation. Dev. Biol. *42*, 160–180.

McInnes, L., Healy, J., and Melville, J. (2018). UMAP: Uniform Manifold Approximation and Projection for Dimension Reduction. arXiv, arXiv:1802.03426 https://arxiv.org/abs/1802.03426.

Méndez-Ferrer, S., Michurina, T.V., Ferraro, F., Mazloom, A.R., Macarthur, B.D., Lira, S.A., Scadden, D.T., Ma'ayan, A., Enikolopov, G.N., and Frenette, P.S. (2010). Mesenchymal and haematopoietic stem cells form a unique bone marrow niche. Nature *466*, 829–834.

Morikawa, S., Mabuchi, Y., Niibe, K., Suzuki, S., Nagoshi, N., Sunabori, T., Shimmura, S., Nagai, Y., Nakagawa, T., Okano, H., and Matsuzaki, Y. (2009a). Development of mesenchymal stem cells partially originate from the neural crest. Biochem. Biophys. Res. Commun. *379*, 1114–1119.

Morikawa, S., Mabuchi, Y., Kubota, Y., Nagai, Y., Niibe, K., Hiratsu, E., Suzuki, S., Miyauchi-Hara, C., Nagoshi, N., Sunabori, T., et al. (2009b). Prospective identification, isolation, and systemic transplantation of multipotent mesenchymal stem cells in murine bone marrow. J. Exp. Med. *206*, 2483–2496.

Nieto, M.A. (2002). The snail superfamily of zinc-finger transcription factors. Nat. Rev. Mol. Cell Biol. *3*, 155–166.

Olsen, B.R., Reginato, A.M., and Wang, W. (2000). Bone development. Annu. Rev. Cell Dev. Biol. *16*, 191–220.

Pardali, E., Sanchez-Duffhues, G., Gomez-Puerto, M.C., and Ten Dijke, P. (2017). TGF-β-induced endothelial-mesenchymal transition in fibrotic diseases. Int. J. Mol. Sci. *18*, 2157.

Patsch, C., Challet-Meylan, L., Thoma, E.C., Urich, E., Heckel, T., O'Sullivan, J.F., Grainger, S.J., Kapp, F.G., Sun, L., Christensen, K., et al. (2015). Generation of vascular endothelial and smooth muscle cells from human pluripotent stem cells. Nat. Cell Biol. *17*, 994–1003.

Piera-Velazquez, S., and Jimenez, S.A. (2019). Endothelial to mesenchymal transition: Role in physiology and in the pathogenesis of human diseases. Physiol. Rev. *99*, 1281–1324.

Pinho, S., Lacombe, J., Hanoun, M., Mizoguchi, T., Bruns, I., Kunisaki, Y., and Frenette, P.S. (2013). PDGFRα and CD51 mark human nestin$^+$ sphere-forming mesenchymal stem cells capable of hematopoietic progenitor cell expansion. J. Exp. Med. *210*, 1351–1367.

Quirici, N., Soligo, D., Bossolasco, P., Servida, F., Lumini, C., and Deliliers, G.L. (2002). Isolation of bone marrow mesenchymal stem cells by anti-nerve growth factor receptor antibodies. Exp. Hematol. *30*, 783–791.

Rafii, S., Butler, J.M., and Ding, B.-S. (2016). Angiocrine functions of organ-specific endothelial cells. Nature *529*, 316–325.

Ramasamy, S.K., Kusumbe, A.P., and Adams, R.H. (2015). Regulation of tissue morphogenesis by endothelial cell-derived signals. Trends Cell Biol. *25*, 148–157.

Ramasamy, S.K., Kusumbe, A.P., Itkin, T., Gur-Cohen, S., Lapidot, T., and Adams, R.H. (2016). Regulation of Hematopoiesis and Osteogenesis by Blood Vessel-Derived Signals. Annu. Rev. Cell Dev. Biol. *32*, 649–675.

Sacchetti, B., Funari, A., Michienzi, S., Di Cesare, S., Piersanti, S., Saggio, I., Tagliafico, E., Ferrari, S., Robey, P.G., Riminucci, M., and Bianco, P. (2007). Self-renewing osteoprogenitors in bone marrow sinusoids can organize a hematopoietic microenvironment. Cell *131*, 324–336.

Sánchez-Duffhues, G., de Vinuesa, A.G., Lindeman, J.H., Mulder-Stapel, A., DeRuiter, M.C., Van Munsteren, C., Goumans, M.J., Hierck, B.P., and Ten Dijke, P. (2015). SLUG is expressed in endothelial cells lacking primary cilia to promote cellular calcification. Arterioscler. Thromb. Vasc. Biol. *35*, 616–627.

Sanchez-Duffhues, G., Orlova, V., and Ten Dijke, P. (2016). In Brief: Endothelial-to-mesenchymal transition. J. Pathol. *238*, 378–380.

Satija, R., Farrell, J.A., Gennert, D., Schier, A.F., and Regev, A. (2015). Spatial reconstruction of single-cell gene expression data. Nat. Biotechnol. *33*, 495–502.

Schepers, K., Hsiao, E.C., Garg, T., Scott, M.J., and Passegué, E. (2012). Activated Gs signaling in osteoblastic cells alters the hematopoietic stem cell niche in mice. Blood *120*, 3425–3435.

Scotti, C., Piccinini, E., Takizawa, H., Todorov, A., Bourgine, P., Papadimitropoulos, A., Barbero, A., Manz, M.G., and Martin, I. (2013). Engineering of a functional bone organ through endochondral ossification. Proc. Natl. Acad. Sci. USA *110*, 3997–4002.

Serafini, M., Sacchetti, B., Pievani, A., Redaelli, D., Remoli, C., Biondi, A., Riminucci, M., and Bianco, P. (2014). Establishment of bone marrow and hematopoietic niches in vivo by reversion of chondrocyte differentiation of human bone marrow stromal cells. Stem Cell Res. (Amst.) *12*, 659–672.

Slukvin, I.I., and Kumar, A. (2018). The mesenchymoangioblast, mesodermal precursor for mesenchymal and endothelial cells. Cell. Mol. Life Sci. *75*, 3507–3520.

Souilhol, C., Harmsen, M.C., Evans, P.C., and Krenning, G. (2018). Endothelial-mesenchymal transition in atherosclerosis. Cardiovasc. Res. *114*, 565–577.

Subramanian, A., Tamayo, P., Mootha, V.K., Mukherjee, S., Ebert, B.L., Gillette, M.A., Paulovich, A., Pomeroy, S.L., Golub, T.R., Lander, E.S., and Mesirov, J.P. (2005). Gene set enrichment analysis: a knowledge-based approach for interpreting genome-wide expression profiles. Proc. Natl. Acad. Sci. USA *102*, 15545–15550.

Suzukawa, M., Koketsu, R., Iikura, M., Nakae, S., Matsumoto, K., Nagase, H., Saito, H., Matsushima, K., Ohta, K., Yamamoto, K., and Yamaguchi, M. (2008). Interleukin-33 enhances adhesion, CD11b expression and survival in human eosinophils. Lab. Invest. *88*, 1245–1253.

Syn, W.K., Jung, Y., Omenetti, A., Abdelmalek, M., Guy, C.D., Yang, L., Wang, J., Witek, R.P., Fearing, C.M., Pereira, T.A., et al. (2009). Hedgehog-mediated epithelial-to-mesenchymal transition and fibrogenic repair in nonalcoholic fatty liver disease. Gastroenterology *137*, 1478–1488.e8.

Szulcek, R., Bogaard, H.J., and van Nieuw Amerongen, G.P. (2014). Electric cell-substrate impedance sensing for the quantification of endothelial proliferation, barrier function, and motility. J. Vis. Exp. (85), 51300.

Takashima, Y., Era, T., Nakao, K., Kondo, S., Kasuga, M., Smith, A.G., and Nishikawa, S. (2007). Neuroepithelial cells supply an initial transient wave of MSC differentiation. Cell *129*, 1377–1388.

Tikhonova, A.N., Dolgalev, I., Hu, H., Sivaraj, K.K., Hoxha, E., Cuesta-Domínguez, Á., Pinho, S., Akhmetzyanova, I., Gao, J., Witkowski, M., et al. (2019). The bone marrow microenvironment at single-cell resolution. Nature *569*, 222–228.

Tormin, A., Li, O., Brune, J.C., Walsh, S., Schütz, B., Ehinger, M., Ditzel, N., Kassem, M., and Scheding, S. (2011). CD146 expression on primary nonhematopoietic bone marrow stem cells is correlated with in situ localization. Blood *117*, 5067–5077.

Trapnell, C., Cacchiarelli, D., Grimsby, J., Pokharel, P., Li, S., Morse, M., Lennon, N.J., Livak, K.J., Mikkelsen, T.S., and Rinn, J.L. (2014). The dynamics and regulators of cell fate decisions are revealed by pseudotemporal ordering of single cells. Nat. Biotechnol. *32*, 381–386.

van Meeteren, L.A., and ten Dijke, P. (2012). Regulation of endothelial cell plasticity by TGF-β. Cell Tissue Res. *347*, 177–186.

Vodyanik, M.A., Yu, J., Zhang, X., Tian, S., Stewart, R., Thomson, J.A., and Slukvin, I.I. (2010). A mesoderm-derived precursor for mesenchymal stem and endothelial cells. Cell Stem Cell *7*, 718–729.

Wang, S.M., Coljee, V.W., Pignolo, R.J., Rotenberg, M.O., Cristofalo, V.J., and Sierra, F. (1997). Cloning of the human twist gene: its expression is retained in adult mesodermally-derived tissues. Gene *187*, 83–92.

Wesseling, M., Sakkers, T.R., de Jager, S.C.A., Pasterkamp, G., and Goumans, M.J. (2018). The morphological and molecular mechanisms of epithelial/endothelial-to-mesenchymal transition and its involvement in atherosclerosis. Vascul. Pharmacol. *106*, 1–8.

Worthley, D.L., Churchill, M., Compton, J.T., Tailor, Y., Rao, M., Si, Y., Levin, D., Schwartz, M.G., Uygur, A., Hayakawa, Y., et al. (2015). Gremlin 1 identifies a skeletal stem cell with bone, cartilage, and reticular stromal potential. Cell *160*, 269–284.

Yang, J., Antin, P., Berx, G., Blanpain, C., Brabletz, T., Bronner, M., Campbell, K., Cano, A., Casanova, J., Christofori, G., et al.; EMT International Association (TEMTIA) (2020). Guidelines and definitions for research on epithelial-mesenchymal transition. Nat. Rev. Mol. Cell Biol. *21*, 341–352.

Zambetti, N.A., Ping, Z., Chen, S., Kenswil, K.J.G., Mylona, M.A., Sanders, M.A., Hoogenboezem, R.M., Bindels, E.M.J., Adisty, M.N., Van Strien, P.M.H., et al. (2016). Mesenchymal Inflammation Drives Genotoxic Stress in Hematopoietic Stem Cells and Predicts Disease Evolution in Human Pre-leukemia. Cell Stem Cell *19*, 613–627.

Zeisberg, E.M., Tarnavski, O., Zeisberg, M., Dorfman, A.L., McMullen, J.R., Gustafsson, E., Chandraker, A., Yuan, X., Pu, W.T., Roberts, A.B., et al. (2007). Endothelial-to-mesenchymal transition contributes to cardiac fibrosis. Nat. Med. *13*, 952–961.

Zhou, B.O., Yue, R., Murphy, M.M., Peyer, J.G., and Morrison, S.J. (2014). Leptin-receptor-expressing mesenchymal stromal cells represent the main source of bone formed by adult bone marrow. Cell Stem Cell *15*, 154–168.

STAR★METHODS

KEY RESOURCES TABLE

REAGENT or RESOURCE	SOURCE	IDENTIFIER
Antibodies		
PE/Cy7 anti-human CD45 antibody, Clone HI30	BioLegend	Cat#304015; RRID:AB_314403
PE anti-human CD271 (NGFR) antibody, Clone ME20.4	BioLegend	Cat#345105; RRID:AB_2282827
Pacific Blue anti-human CD235a (Glycophorin A) antibody, Clone HI264	BioLegend	Cat#349108; RRID:AB_11218988
APC/Cyanine7 anti-human CD31 antibody, Clone WM59	BioLegend	Cat#303119; RRID:AB_10643590
FITC anti-human CD9 antibody, Clone HI9a	BioLegend	Cat#312104; RRID:AB_2075894
CD105 (Endoglin) Monoclonal Antibody (SN6), APC	ebioscience	Cat#17-1057-42; RRID:AB_1582211
V450 Mouse Anti-Human CD144, Clone 55-7H1	BD Biosciences	Cat#561569; RRID:AB_10717124
Alexa Fluor® 700 anti-human CD34 antibody, Clone 581	BioLegend	Cat#343525; RRID:AB_2561494
Brilliant Violet 510 anti-human CD45, Clone HI30	BioLegend	Cat#304035; RRID:AB_2561383
PE/Cy7 anti-human CD235a (Glycophorin A) antibody, Clone HI264	BioLegend	Cat#349111; RRID:AB_2562707
APC/Cyanine7 anti-mouse CD45.2 antibody, Clone 104	BioLegend	Cat#109824; RRID:AB_830789
Brilliant Violet 510 anti-mouse TER-119/Erythroid Cells antibody, Clone TER-119	BioLegend	Cat#116237; RRID:AB_2561661
PE/Cy7 anti-mouse CD144 (VE-cadherin) antibody, Clone BV13	BioLegend	Cat#138015; RRID:AB_2562885
Biotin anti-mouse CD51 antibody, Clone RMV-7	BioLegend	Cat#104103; RRID:AB_313072
PE anti-mouse CD51 antibody, Clone RMV-7	BioLegend	Cat#104105; RRID:AB_313074
Pacific Blue anti-mouse Ly-6A/E (Sca-1) antibody, Clone D7	BioLegend	Cat#108120; RRID:AB_493273
CD140a (PDGFRA) Monoclonal Antibody (APA5), APC, Clone APA5	eBioscience	Cat#17-1401-81; RRID:AB_529482
APC-R700 Rat Anti-Mouse CD31, Clone MEC 13.3	BD Biosciences	Cat#565509; RRID:AB_2739273
FITC anti-human CD271 (NGFR) antibody, Clone ME20.4	BioLegend	Cat#345103; RRID:AB_1937226
Anti-NGFR antibody produced in rabbit	Sigma-Aldrich	Cat#HPA004765; RRID:AB_1079233
Human Endoglin/CD105 Affinity Purified Polyclonal Ab antibody	R&D Systems	Cat#AF1097; RRID:AB_354598
Donkey anti-Rabbit IgG (H+L) Highly Cross-Adsorbed Secondary Antibody, Alexa Fluor 488	Thermo Fisher Scientific	Cat#A-21206; RRID:AB_2535792
Cy3 AffiniPure Donkey Anti-Goat IgG (H+L) antibody	Jackson ImmunoResearch Labs	Cat#705-165-147; RRID:AB_2307351
Mouse Anti-CD31 Monoclonal Antibody, Unconjugated, Clone JC70	Cell Marque	Cat#131M-94; RRID:AB_1516761
CD105 antibody	GeneTex	Cat#GTX100508; RRID:AB_1950199
UltraMap anti-Ms HRP (RUO), DISCOVERY	Ventana	Cat#760-4313
Anti-Rabbit HQ, DISCOVERY	Ventana	Cat#760-4815
Anti-HQ HRP, DISCOVERY	Ventana	Cat# 760-4820
PE-Cy7 Mouse Anti-Human CD34, Clone 8G12	BD Biosciences	Cat#327907; RRID:AB_94055
FITC anti-human CD51 antibody, Clone NKI-M9	BioLegend	Cat#327907; RRID:AB_940558
PE anti-human CD73 (Ecto-5′-nucleotidase) antibody	BioLegend	Cat#344003; RRID:AB_1877224
CD90 (Thy-1) Monoclonal Antibody (eBio5E10 (5E10)), PE	Thermo Fisher Scientific	Cat#12-0909-42; RRID:AB_10670624

(*Continued on next page*)

Continued

REAGENT or RESOURCE	SOURCE	IDENTIFIER
Mouse Anti-Human CD146 Monoclonal Antibody, PE Conjugated, Clone P1H12	BD Biosciences	Cat#561013; RRID:AB_2033941
APC/Cyanine7 Mouse IgG1, κ Isotype Ctrl Antibody	BioLegend	Cat#400127
FITC Mouse IgG1, κ Isotype Ctrl Antibody	BioLegend	Cat#400107
PE Mouse IgG1, κ Isotype Ctrl Antibody	BioLegend	Cat#400111
PE/Cyanine7 Mouse IgG1, κ Isotype Ctrl Antibody	BioLegend	Cat#400125
Mouse IgG1 kappa Isotype Control (P3.6.2.8.1), APC, eBioscience antibody	Thermo Fisher Scientific	Cat#17-4714-41; RRID:AB_1603319
FITC Rat Anti-Mouse CD44, Clone IM7	BD Biosciences	Cat#553133; RRID:AB_2076224
CD29 (Integrin beta 1) Monoclonal Antibody (eBioHMb1-1 (HMb1-1)), eFluor 450, eBioscience	Thermo Fisher Scientific	Cat#48-0291-80; RRID:AB_11217874
APC/Cyanine7 anti-mouse/human CD11b Antibody, Clone M1/70	BioLegend	Cat#101226; RRID:AB_830642
CD34 PE-Cy7 CE antibody	BD Biosciences	Cat#348811 RRID:AB_2868855
Pacific Blue anti-human CD45 antibody	BioLegend	Cat#304022; RRID:AB_493655
Human Hematopoietic Lineage Antibody Cocktail, FITC	eBiosciences	Cat#22-7778-72; RRID:AB_1311229
Mouse Anti-Human CD38 Monoclonal Antibody, PerCP-Cy5.5 Conjugated, Clone HIT2	BD Biosciences	Cat#561106; RRID:AB_2033958
Mouse Anti-Human CD45RA Monoclonal Antibody, APC-H7 Conjugated, Clone HI100	BD Biosciences	Cat#560674; RRID:AB_1727497
Recombinant HRP Anti-GAPDH antibody	Abcam	Cat#EPR6256
goat anti-rabbit biotinylated link	Biogenex Laboratories	Cat#HK-326-UR
Alkaline phosphatase-labeled antibody	Biogenex Laboratories	Cat#HK-321-UK
Purified anti-mouse CD45 antibody, Clone 30-F11	BioLegend	Cat#103101; RRID:AB_312966
Anti-Rat IgG (H+L), made in rabbit antibody	Vector Laboratories	Cat#BA-4000; RRID:AB_2336206
APC anti-human CD31 antibody, Clone WM59	BioLegend	Cat#303115; RRID:AB_1877152
APC anti-mouse/human CD44 antibody, Clone IM7	BioLegend	Cat#103011; RRID:AB_312962
Mouse Anti-Human IgG1, k Isotype Control, V450 Conjugated antibody	BD Biosciences	Cat#560373; RRID:AB_1645606
VE-Cadherin Antibody	Cell Signaling	Cat#2158
Mouse Anti-Human Fibronectin Monoclonal Antibody, Unconjugated, Clone FN-15	Sigma-Aldrich	Cat#F7387; RRID:AB_476988
Mouse Anti-Actin, alpha-Smooth Muscle Monoclonal Antibody, Unconjugated, Clone 1A4	Sigma-Aldrich	Cat#A2547; RRID:AB_476701
Fluorescein (FITC) AffiniPure Goat Anti-Mouse IgG (H+L)	Jackson ImmunoResearch Labs	Cat#115-095-003; RRID:AB_2338589
Goat anti-Rabbit IgG (H+L) Highly Cross-Adsorbed Secondary Antibody, Alexa Fluor Plus 555	Thermo Fisher Scientific	Cat#A32732; RRID:AB_2633281
Cy3-AffiniPure Goat Anti-Mouse IgG (H+L) antibody	Jackson ImmunoResearch Labs	Cat#115-165-003; RRID:AB_2338680
Biological samples		
Bone marrow aspirates from healthy individuals	Erasmus MC, Rotterdam	N/A
Bone marrow aspirates from AML day 17 patients	Erasmus MC, Rotterdam	N/A
Fetal bone	Erasmus MC, Rotterdam; AMC, Amsterdam	N/A
Adult bone (hip replacement surgery)	Erasmus MC, Rotterdam	N/A
Chemicals, peptides, and recombinant proteins		
Collagenase Type I (0.25%)	Stem Cell	Cat#07902
Lysing Solution IOTest 3 10X Concentrate	Beckman Coulter	Cat#A07799
Streptavidin, Alexa Fluor 488 conjugate	Thermo Fisher Scientific	Cat#S11223
7-AAD Viability Dye	Beckman Coulter	Cat#A07704

(*Continued on next page*)

Continued

REAGENT or RESOURCE	SOURCE	IDENTIFIER
VECTASHIELD® Antifade Mounting Medium with DAPI	Vector Laboratories	Cat#H-1200-10
DISCOVERY CC1	Ventana	Cat# 950-500
Red 610 Kit. DISCOVERY	Ventana	Cat#760-245
Cell Conditioning 2 (CC2)	Ventana	Cat#950-123
Cy5 Kit, DISCOVERY	Ventana	Cat#760-238
FAM Kit, DISCOVERY	Ventana	Cat#760-243
Fluorescence Mounting Medium	Agilent DAKO	Cat#S3023
Recombinant Murine FGF-basic	PeproTech	Cat#450-33
Recombinant Murine EGF	PeproTech	Cat#315-09
β-Glycerophosphate disodium salt hydrate	Sigma-Aldrich	Cat#G6376
Dexamethasone	Sigma-Aldrich	Cat#D4902
L-Ascorbic acid 2-phosphate sesquimagnesium salt hydrate	Sigma-Aldrich	Cat#A8960
Corning® ITS+ Premix Universal Culture Supplement	Corning	Cat#354352
L-Proline	Sigma-Aldrich	Cat#P5607
Sodium Pyruvate	Fisher Scientific	Cat#11530396
Indomethacin	Sigma-Aldrich	Cat#I7378
Insulin solution human	Sigma-Aldrich	Cat#I9278
3-Isobutyl-1-methylxanthine	Sigma-Aldrich	Cat#I5879
Recombinant Human TGF-beta 1 Protein	R&D Systems	Cat#240-B
Recombinant Human TGF-beta 3 Protein	R&D Systems	Cat#243-B3
Alizarin Red S	Sigma-Aldrich	Cat#A5533
Oil Red O solution	Sigma-Aldrich	Cat#O1391
Thionin acetate salt	Sigma-Aldrich	Cat#T7029
Toluidine Blue	Sigma-Aldrich	Cat#89640
Nuclear Fast Red solution	Sigma-Aldrich	Cat#N3020
Interleukin-33 Human Recombinant	Prospec	Cat#CYT-425
Recombinant Human SCF	CellGenix	Cat#1018
Recombinant Human TPO	CellGenix	Cat#1017
Recombinant Human Flt-3L	CellGenix	Cat#1015
Flow-Count Fluorospheres	Beckman Coulter	Cat#7547053
MethoCult GF H84434	StemCell Technologies	Cat#84434
Collagen human	Sigma-Aldrich	Cat#C7624
Hematoxylin	Vector Laboratories	Cat#H-3401-500
VectaMount AQ Mounting Medium	Vector Laboratories	Cat#H-5501
ProLong Gold Antifade Mountant with DAPI	Thermo Fisher Scientific	Cat#P36931
Critical commercial assays		
SMART-Seq® v4 Ultra® Low Input RNA Kit for Sequencing	Takara	Cat#634891
Agilent High Sensitivity DNA Kit	Agilent	Cat#5067-4626
Chromium Single Cell 3′ Reagent Kits v3	10X Genomics	Cat#PN-1000075
Macherey-Nagel NucleoSpin RNA	Fisher Scientific	Cat#NC9581114
RevertAid First Strand cDNA Synthesis Kit	Thermo Scientific	Cat#K1621
Avidin/Biotin blocking kit	Vector Laboratories	Cat#SP-2001
ABC-HRP kit	Vector Laboratories	Cat#PK-6100
DAB Substrate kit	Vector Laboratories	Cat#SK-4100

(*Continued on next page*)

Continued		
REAGENT or RESOURCE	SOURCE	IDENTIFIER
Deposited data		
Bulk RNA sequencing of LNGFR^{+} hRECs, endothelial (LNGFR^{-} hRECs) and stromal (CD31^{-}LNGFR^{+}) FACS-purified cells from fetal bone	EGA	EGAS00001004946
Single cell RNA-sequencing of murine endothelial and stromal populations at embryonic day 17 (E17)	Array Express	E-MTAB-9994
Bulk RNA sequencing of endothelial-derived and non-endothelial-derived BMSCs and OLCs of VE-Cadherin-Cre;LoxP-tdTomato mice (3/11 week-old)	Array Express	E-MTAB-10020
Experimental models: organisms/strains		
C57BL/6J	The Jackson Laboratory	Cat#000664; RRID:IMSR_JAX:000664
BALB/cAnNCrl	Charles River Laboratories	Strain Code: 028
VE-Cadherin-Cre (B6;129-Tg(Cdh5-cre)1Spe/J)	The Jackson Laboratory	Cat#017968; RRID:IMSR_JAX:017968
Rosa26-tdTomato (B6.Cg-Gt(ROSA)26Sortm9 (CAG-tdTomato)Hze/J)	The Jackson Laboratory	Cat#007909; RRID:IMSR_JAX:007909
Oligonucleotides		
See Table S4		
Software and algorithms		
GraphPadPrism (v8)	GraphPad Software Inc	RRID:SCR_002798
FlowJo (v10)	Tree Star Inc	RRID:SCR_008520
Adobe Illustrator CC 2018	Adobe Systems Inc.	RRID:SCR_010279
Leica Application Suite X	Leica Microsystems	RRID:SCR_013673
IBM SPSS Statistics 24	IBM	https://www.ibm.com/support/pages/downloading-ibm-spss-statistics-24
DESeq2 package	Love et al., 2014	http://bioconductor.org/packages/release/bioc/html/DESeq2.html
CellRanger (v 3.0.2)	10x Genomics	https://support.10xgenomics.com/single-cell-gene-expression/software/release-notes/3-0
R (v3.6.1)	CRAN	https://cran.r-project.org/bin/windows/base/old/3.6.1/
Seurat (v 3.1.0)	Satija et al., 2015	https://satijalab.org/seurat/install.html
biomaRt package (v 2.42.0)	Durinck et al., 2009	https://bioconductor.org/packages/release/bioc/html/biomaRt.html
GSEA (v4.0.3)	Subramanian et al., 2005	http://www.gsea-msigdb.org/gsea/index.jsp
Monocle (v2.12.0)	Trapnell et al., 2014	http://cole-trapnell-lab.github.io/monocle-release/docs/

RESOURCE AVAILABILITY

Lead contact

Further information and requests for resources and reagents should be directed to and will be fulfilled by the Lead Contact, Marc Raaijmakers (m.h.g.raaijmakers@erasmusmc.nl).

Materials availability

This study did not generate new unique reagents. For specific details on availability please refer to the Key resources table.

Data and code availability

The datasets generated during this study are available at EGA with accession number EGAS00001004946 and at Array Express with accession numbers E-MTAB-9994 and E-MTAB-10020.

EXPERIMENTAL MODEL AND SUBJECT DETAILS

Animal models

For subcutaneous implantation of chondrogenically primed pellets, BALB/cAnNCrl male mice at 8 weeks of age were purchased from Charles River. Animal experiments were conducted in the animal facility of the Erasmus MC with approval of the animal ethics committee (project license AVD1010020186166).

For lineage tracing experiments, *VE-Cadherin-Cre (B6;129-Tg(Cdh5-cre)1Spe/J)* mice (Chen et al., 2009), and *Rosa26-tdTomato (B6.Cg-Gt(ROSA)26Sortm9(CAG-tdTomato)Hze/J)* mice (Madisen et al., 2010) were obtained from The Jackson Laboratory and intercrossed to generate *VE-Cadherin-Cre;LoxP-tdTomato* mice. Experimental mice were analyzed at 3 and 11 weeks of age.

For the isolation and scRNaseq of stromal cells and ECs from murine fetal bones, a C57BL/6J female mouse was purchased from Charles River and bred in-house.

Animals were maintained in specific pathogen-free conditions in the Experimental Animal Center of Erasmus MC (EDC). Mice were housed in groups of maximum four animals under a standard 12 h light/dark cycle, with access to food and water *ad libitum*. All mice were euthanized by cervical dislocation. Animal studies were approved by the Animal Welfare/Ethics Committee of the EDC in accordance with legislation in the Netherlands.

Human subjects

Human bone samples (BM) were collected as previously described (Kenswil et al., 2018). Briefly, BM aspirates of AML patients were collected 17 days after start of chemotherapy (median age: 65 years, range 28-76). All patients were in complete remission after the first cycle of chemotherapy. Control BM was collected by aspiration from healthy individuals that served as donors for allogeneic bone marrow transplantation (median age: 44 years, range 24-58). Bone marrow aspirate with a total volume of 10-30 mL were obtained by Jamshidi needles with repositioning. Bone tissue was obtained from patients undergoing hip replacement surgery (median age: 55 years, range 22-71). Human fetal long bones (median age: 18 gestational weeks, range 15-20) were collected from elective abortions. Gestational age was confirmed by ultrasonic measurement by determining skull diameter and femoral length. The use of human fetal and postnatal tissues was approved by the Medical Ethical Commissions of the Academic Medical Center of Amsterdam and the Erasmus University Medical Center of Rotterdam, the Netherlands, in accordance with the declaration of Helsinki with informed consent.

Primary cultures

Human stromal cells derived from FACS-sorted fetal LNGFR$^+$ ECs and CD31$^-$LNGFR$^+$ BMSCs were cultured in EGM-2 medium until passage 2 and then transferred to αMEM medium containing 10% FCS and 1% penicillin/streptomycin. Cells were subsequently collected at indicated passages for FACS-analyses, differentiation assays and cryopreservation.

BMSCs from *VE-Cadherin-Cre;LoxP-tdTomato* mice were obtained by culturing 5x10^5 whole lysed unfractionated BM cells/cm^2 in αMEM medium containing 20% FCS and 1% penicillin/streptomycin until reaching confluency and collected for flow cytometry analysis.

BMSCs from collagenase-digested bone chips of *VE-Cadherin-Cre;LoxP-tdTomato* mice were obtained by placing the bone chips in a 15 cm dish for adherent cells with 25 mL αMEM medium containing 10% FBS, mesenchymal stem cell-qualified (GIBCO), 1% penicillin/streptomycin, 1 ng/ml murine basic FGF (Peprotech) and 5 ng/ml murine EGF (Peprotech). After 72 hours, bone chips were transferred to a new 15 cm plate with 25 mL of medium. Fresh medium was added on top after 7 days. When confluent (±14 days), cells were detached from the plate using TrypLE Select (1X), no Phenol Red (GIBCO) and FACS-purified to remove hematopoietic contamination using the following antibodies: anti-CD45.2 (1:100, Biolegend) and anti-CD11b (1:100, Biolegend).

Human umbilical vein endothelial cells (HUVECs) were isolated as described elsewhere (Crampton et al., 2007) and cultured in EBM-2 medium with 10% FBS on 1% w/v gelatin or endothelial cell medium (ECM) consisting of RPMI 1640 basal medium (Lonza) with heat inactivated Fetal Bovine Serum (Lonza, 20% v/v), Heparin (LEO, 5U/ml), EC Growth Factor (ECGF; own preparation 50 μg/ml) (Lerner and Harrison, 1990), penicillin/streptomycin (GIBCO, 1%v/v) and L-Glutamine (Lonza, 2nM), when indicated.

ECFCs were generated from 30-60 mL of peripheral blood collected in citrate-treated collection tubes, after first obtaining written informed consent in accordance with institutional guidelines. The first 2 mL of blood were discarded to avoid contamination with skin fibroblasts. The blood was pre-diluted 1:1 with pre-warmed PBS and centrifuged at 740 x g for 30 min in the presence of Ficoll Paque Plus (GE Healthcare Europe GmbH), in order to separate a fraction containing mononuclear cells (MNCs). MNCs were subsequently collected and washed three times with M199 (Lonza) supplemented with 0.1% penicillin/streptomycin (Invitrogen). Next, these cells were re-suspended in complete EBM-2 (Lonza) supplemented with 10% platelet lysate (PL-EGM) and 0.1% penicillin-streptomycin, and seeded at a density of 1.3 × 10^6 cells/cm^2 into 48 well-plates pre-coated with 3 μg/cm^2 human collagen type I prepared according to manufacturer's. After 24 hours, non-adherent cells were carefully removed and fresh medium was added to each well. From this moment, the medium was replaced every day while supernatants were discarded. ECFCs colonies with regular cobblestone morphology appeared within 3-4 weeks. Once confluent, these cells are progressively adapted to and cultured in EBM-2 medium with 10% FBS on 1% w/v gelatin.

All cells were cultured at 37°C, 5% CO_2.

METHOD DETAILS

Human bone (marrow) cell isolation

Mononuclear cells (MNCs) were isolated from human BM aspirates as previously reported (Kenswil et al., 2018). Briefly, AML Day 17 BM aspirates were mixed 1:25 with red blood cell lysis solution (NH4Cl 0.155 M, KHCO3 0.01 M, EDTA-Na2.2H2O 0.1 M, pH 7.4) to lyse red blood cells. Cryopreserved BM aspirates from healthy individuals were thawed in a waterbath at 37°C. MNCs were collected by centrifugation and washed once with phosphate buffered saline (PBS)+0.5% fetal calf serum (FCS).

Fetal BM MNCs were isolated from fetal long bones, which were first cut into smaller pieces before being gently crushed using a mortar and pestle. BM fraction was filtered through a 40-μm filter and collected in a 50 mL collection tube. Resulting bone fragments were digested with 0.25% collagenase type I (Stem Cell) for 45 minutes in a waterbath at 37°C to release fetal bone cells. Subsequent BM and bone fragment cell suspensions were washed in PBS + 0.5% FCS and cleared from erythrocytes with IOtest3 lysing solution (Beckman Coulter). This was then followed by another washing step with PBS + 0.5%FCS. For adult hip bone cells, trabecular bone was also gently crushed using a mortar and pestle and resulting BM and collagenased bone fractions were processed as described for fetal bone cells.

Fluorescence-activated cell sorting (FACS) of human niche cells

Cell sorting was performed as previously described (Kenswil et al., 2018). Cells were stained with the following antibodies using optimized dilutions: CD45 (clone HI30, 1:100), CD271 (clone ME20.4, 1:100), CD235a (clone HI264, 1:100), CD31 (clone WM59, 1:100), CD9 (clone HI9a, 1:100) all from Biolegend, and CD105 (clone SN6, 1:50) from eBioscience, and subsequently sorted using a FACS ARIAIII Cells Sorter (BD Biosciences). For bulk-RNASeq, cells were directly sorted in 800μl Trizol (Ambion) for RNA isolation.

In addition, to determine CD34 and CD144 expression, a number of fetal BM samples were also stained with the following antibodies: CD144 (clone 55-7H1, 1:50) from BD Biosciences, and CD34 (clone 581, 1:100) from Biolegend.

Immunocytochemistry to detect CD31, CD105, and CD271 on human niche cells

To detect CD31, CD105, and CD271 expression on individual niche cells, $CD31^+$ and $CD31^-$ cells were sorted in PBS + 0.5% FCS and subsequently transferred to poly-l-lysine coated glass slides. To prevent interference from FACS antibodies directed against CD9 and CD105, we excluded these and used the following antibody cocktail for sorting: CD45 (clone HI30, 1:100), CD235a (clone HI264, 1:100), CD271 (clone ME20.4, 1:100), and CD31 (clone WM59, 1:100), all from Biolegend, and 7AAD to exclude dead cells.

FACS-sorted niche cells were fixed with 4% paraformaldehyde (PFA)/PBS for 15 minutes on ice, were washed 3 times with PBS, and then incubated in 1%BSA/PBS for 1 hour at room temperature to block non-specific binding sites. Next, cells were stained with rabbit anti-human CD271 (Sigma-Aldrich) and goat anti-human CD105 antibodies (R&D Systems). Secondary staining was performed using Alexa Fluor 488-conjugated donkey anti-rabbit (Thermo Fisher Scientific), and Cy3-conjugated donkey anti-goat antibodies (Jackson ImmunoResearch Labs). After 2 washes in PBS, slides were mounted in VECTASHIELD Mounting Medium with DAPI (Vector Laboratories).

Images were acquired with a Leica TCS SP5 confocal microscope using the LAS software (Leica Microsystems). Alexa Fluor 488 was detected with the 488 laser, Cy3 was detected using the 561 laser, and CD31-APC/Cy7 was detected by using the 633 laser.

Multiplex immunofluorescence staining to detect CD31, CD105 and CD271 in fetal bone

To determine the localization of triple positive cells in fetal bone, 4-μm-thick sections of paraffin embedded formalin-fixed femurs were cut and staining with CD31 (Cell Marque), CD105 (Genetex) and CD271 (Sigma-Aldrich) was performed by automated multiplex IF using the Ventana Benchmark Discovery (Ventana Medical Systems Inc.). All antibodies were used at a concentration of 2.5 μg/ml. Following deparaffinization and heat-induced antigen retrieval with CC1 (Ventana) at 97°C for 40 minutes, the tissue samples were incubated first with CD31 for 32 minutes at 37°C followed by secondary antibody UMAP goat-anti-mouse HRP (Ventana) for 16 minutes at 37°C and detected with Red610 (Ventana). Antibody denaturation step was performed using CC2 (Ventana) for 8 minutes at 100°C. Second, CD105 was incubated for 32 minutes at 37°C followed secondary antibody rabbit HQ (Ventana) and anti-HQ HRP (Ventana) and detected with Cy5 (Ventana). Antibody denaturation step was performed using CC2 for 8 minutes at 100°C. Third, CD271 was incubated for 32 minutes at 37°C followed by secondary antibody rabbit HQ and anti-HQ HRP and detected with FAM (Ventana). Slides were washed in PBS containing DAPI and covered with anti-fading medium (DAKO). Images were acquired with a Leica TCS SP5 confocal microscope using the LAS software (Leica Microsystems).

Bulk-RNA Sequencing and gene set enrichment analysis (GSEA)

RNA of sorted cells was extracted using TRIzol reagent (Invitrogen) according to the manufacturer's instructions for RNA, in combination isolation with GenElute LPA (Sigma-Aldrich). cDNA was prepared using SMARTer procedure with the SMART-Seq v4 Ultra Low Input RNA Kit (Clontech) for Illumina Sequencing. The Agilent 2100 Bio-analyzer and the High Sensitivity DNA kit were applied to determine the quantity and quality of the cDNA production. Library preparation and RNA-sequencing was performed as previously described and validated for low cell number-input (Chen et al., 2016b). In brief, prior to sequence alignment, the SMARTer adapters were trimmed using the cutadapt program. The resulting sequences were aligned to the human or murine RefSeq transcriptome using STAR. Sequences that could not be aligned to the RefSeq transcriptome were aligned to the reference genome (build hg19 and mm10 for mice). Normalization and quantification were performed using Cufflinks. The resulting gene expression values are

measured as FPKM (Fragments per kilobase of exon per million fragments mapped). Fragment counts were determined per gene with HTSeq-count, utilizing union modes, and subsequently used for differential expression analysis using the DESeq2 package, with standard parameters, in the R environment. Multiple testing correction was performed with the Benjamini-Hochberg procedure to control the False Discovery Rate (FDR). Principle component analysis was performed on the fragment counts using the R environment. Finally, gene set enrichment analysis (GSEA) was performed on the FPKM values using the curated C2 collection of gene sets within MSigDB (Subramanian et al., 2005). Similarly, Gene-ontology (GO) analysis was performed using the curated C5 collection of gene sets.

Human stromal cell flow cytometry analysis

Stromal cells derived from FACS-sorted fetal LNGFR$^+$ ECs and CD31$^-$LNGFR$^+$ BMSCs were cultured and collected at P2 and P4, and stained with the following antibodies using optimized dilutions: CD31 (clone WM59, 1:100), CD45 (clone HI30, 1:50), CD51 (clone NKI-M9, 1:100), CD73 (clone AD2, 1:100) all from Biolegend, CD34 (clone 8G12, 1:50) and CD146 (clone P1H12, 1:100) from BD Biosciences, CD90 (clone eBio5E10, 1:100) and CD105 (clone SN6, 1:50) from eBioscience.

Cells were also separately incubated with appropriate mouse IgG1, kappa isotype controls: APC/Cy7, FITC, PE, PE/Cy7, all from Biolegend, and APC from eBioscience. Flow-cytometric analysis was performed using a BD LSRII (BD Biosciences) and data were analyzed using FlowJo (Tree Star Inc).

Fibroblast colony-forming efficiency assay

FACS-sorted fetal LNGFR$^+$ hRECs and CD31$^-$LNGFR$^+$ BMSCs were seeded in EGM-2 medium (Lonza) supplemented with EGM-2 SingleQuot growth factors (Lonza), 1 cell per well in a 96-well plate at 37°C and 5% CO_2. After 2 weeks, cells were fixed with 70% ethanol (vol/vol) and stained with Giemsa. CFU-F colonies were enumerated as previously described (Kenswil et al., 2018).

Co-culture of hematopoietic stem/progenitor cells with the stromal progeny of LNGFR$^+$ ECs and CD31$^-$LNGFR$^+$ BMSCs

Isolation of hematopoietic progenitor/stem cells (HSPCs) from umbilical cord blood (CB) was performed as previously described (Kenswil et al., 2018). Briefly, CD34$^+$ CB cells were isolated using a Ficoll gradient protocol and by magnetic-activated cell sorting (MACS). 24 hours prior to co-culture, to establish a stromal feeder layer, 2 × 10^4 stromal cells were seeded per well in a 48-well plate in triplicate. Next, 7.5 × 10^3 HSPCs were seeded on the feeder layers per well and cultured in 350 μl α-MEM containing 10% FCS supplemented with human SCF (25 ng/ml), TPO (25 ng/ml), FLT3L (25 ng/ml), all from Cellgenix, at 37°C and 5% CO_2. Medium was refreshed every 3-4 days and cells collected at day 7 for FACs analysis and hematopoietic colony forming-unit (CFU-C) assays, as previously described (Kenswil et al., 2018).

Quantification and multiparametric immunophenotyping of cultured HSPCs

Subsequently, total cell number was quantified by the single-method platform flow cytometric assay (Kenswil et al., 2018). Supernatant containing the non-adherent cultured HSPCs was collected after gentle resuspension and were mixed with adherent cells obtained by dissociation using TrypLE Select (1X), no Phenol Red (GIBCO). Cells were then incubated with CD34 (1:50, BD Biosciences) and CD45 (1:50, Biolegend) antibodies to identify HSPCs, and a calibrated number of flow-count fluorosphere beads (Beckman Coulter). 7AAD was also included to distinguish between living and non-living cells. The total number of living MNC per μl (n) in a well was calculated using the following formula: n = ((number of MNC events recorded * bead concentration)/ number of recorded single beads)/ (volume cells/ volume beads).

Similarly, the immunophenotype of the cells was determined by staining the cells with hematopoietic lineage-marker cocktail (1:12.5), CD90 (clone eBio5E10, 1:50) both from eBiosciences, and CD34 (clone 8G12, 1:50), CD38 (clone HIT2, 1:30), and CD45RA (clone HI100, 1:50) all from BD Biosciences. Living cells were identified by excluding 7AAD$^+$ cells. Flow cytometric analysis was performed using a BD LSRII (BD Biosciences) and data were analyzed using FlowJo (Tree Star Inc).

Human hematopoietic colony forming-unit assay

To further assess the hematopoietic potential of cultured HSPCs following co-culture with stromal progeny of LNGFR$^+$ ECs or CD31$^-$LNGFR$^+$ BMSCs, we performed a colony-forming unit assay (CFU-C). Input equivalent of 1 × 10^3 cultured CD34$^+$ cells of each condition (LNGFR$^+$ ECs versus CD31$^-$LNGFR$^+$ BMSCs) was resuspended in 400 μL Iscove's Modified Dulbecco's Medium (IMDM) and transferred to 3.6 mL of methylcellulose (MethoCult, StemCell Technologies). Cells were then plated in triplicate in 1 cm^2 Petri-dishes (1 ml/dish) and were kept at 37°C, 5% CO_2. Colonies were counted after 12-14 days.

Subcutaneous implantation of chondrogenically primed pellets containing LNGFR$^+$ ECs-derived stromal cells

Stromal cells derived from LNGFR$^+$ ECs were seeded in 15 ml-polypropylene conical tube and centrifuged to form 3D pellets (2 × 10^5 cells/pellet). The pellets were cultured in 500 μL DMEM-high-glucose GlutaMAX+ (GIBCO) supplemented with 1.5 μg/ml fungizone, 50 μg/ml gentamicin, 1% ITS+ Premix (Corning), 40 μg/ml L-proline (Sigma-Aldrich), 1 mM sodium pyruvate (GIBCO), 100 nM dexamethasone (Sigma-Aldrich), 25 μg/ml L-ascorbic acid-2-phosphate and 10 ng/ml TGF-β3 (R&D Systems) for 3 weeks. The culture medium was renewed twice a week.

Next, these pellets were implanted subcutaneously on the dorsum of 8 weeks old male athymic nude mice (BALB/cAnNCrl; Charles River). 1h before implantation, animals were given pain medication (buprenorphine, 0.05 mg/kg body weight). Following induction of general anesthesia (isoflurane), four transverse incisions were created in the skin of the dorsum: two between the shoulder blades and two at the level of the hips. Four subcutaneous pockets were created by blunt dissection and a construct consisting of 6 chondrogenically primed hREC pellets was implanted in each pocket (n = 6 constructs). The incisions were closed with staples. 10 weeks post-implantation, pellet mineralization was assessed by Micro-computed tomography (μCT) imaging. μCT scans were performed and reconstructed with the Quantum GX-2 imaging systems (PerkinElmer), using a field of view of 86 mm (90 kV/88 uA, 4 min). Animals were euthanized by cervical dislocation and the constructs were carefully retrieved.

Histological analysis and immunohistochemistry of 3D pellets

In vitro chondrogenically primed pellets and *in vivo* bone constructs were fixed for 24h in 4% (w/v) formaldehyde in PBS. *In vivo* samples were further decalcified for 7d in 10% w/v EDTA in PBS, changing the solution twice per week. Next, samples were embedded in paraffin wax. 6 μm-thick sections were cut, deparaffinized, rehydrated and stained with hematoxylin and eosin (H&E) or 0.04% thionin solution (Sigma-Aldrich) to detect glycosaminoglycans (GAGs), or 0.4% toluidine blue solution (Sigma-Aldrich).

Immunohistochemistry for human glyceraldehyde-3-phosphate dehydrogenase (hGAPDH)

After deparaffinization and rehydration, antigen retrieval was performed by placing the slides in 95°C Tris-EDTA buffer pH 6 for 25 min. Blocking of non-specific binding was performed with 10% goat serum (Southern Biotech) in TBS + 1% BSA (Sigma-Aldrich) 1% milk powder for 30 min. Next, the sections were incubated for 1h with a primary antibody against hGAPDH (rabbit anti-human, 0.2 μg/ml dilution; Abcam), followed by 30 min incubation with a biotinylated link (goat anti-rabbit; Biogenex Laboratories). Next, an alkaline phosphatase-labeled antibody was used (Biogenex Laboratories), which in combination with the Neu Fuchsine substrate resulted in a red staining. An isotype IgG1 monoclonal antibody was used as negative control for the staining. Following light counterstaining with hematoxilin, the sections were mounted in VectaMount AQ mounting medium (Vector Laboratories).

Immunohistochemistry for mouse CD45 (mCD45)

After deparaffinization and rehydration, antigen retrieval was performed with Proteinase K treatment (50μg/ml in dH2O) for 15 minutes at room temperature. Peroxidases were blocked by incubating sections for 10 minutes in 3% H2O2/methanol. Sections were blocked for non-specific binding using Avidin/Biotin blocking kit (Vector Laboratories) followed by normal serum blocking (5% mouse, 5% human and 5% rabbit). Sections were stained with anti-CD45 antibody in a 1:50 dilution (clone 30-F11, Biolegend) for 1 hour at room temperature. Secondary staining was preformed using a rabbit anti-rat IgG biotinylated antibody in a 1:500 dilution (Vector Laboratories) for 30 minutes at room temperature. Staining was visualized using the ABC-HRP kit (Vector Laboratories) and DAB Substrate kit (Vector Laboratories). Sections were counterstained with Hematoxylin (Vector Laboratories).

Isolation and ScRNaseq of stromal cells and ECs from murine fetal bone

To isolate stromal and endothelial cells from fetal bone, 9 fetuses were collected from a pregnant C57BL/6J mouse euthanized by cervical dislocation at day 17 of gestation (E17). Fetal long bones were dissected and cleaned using a dissection microscope. Collagenased bone fraction and bone marrow were obtained as previously described (Zambetti et al., 2016) and cell suspensions were stained using the following antibodies: anti-CD45.2 (clone 104, 1:100), anti-Ter119 (clone TER-119, 1:50), anti-CD51 (clone RMV-7, 1:50), anti-CD144 (clone BV13, 1:200), anti-Sca1 (clone D7, 1:100) all from Biolegend and anti-CD31 (Clone MEC 13.3, 1:100) from BD Biosciences. To discriminate between live and dead cells, staining with the viability dye 7-AAD (1:100) was performed. Endothelial cell enriched cell populations (7AAD- CD45- Ter119- CD31+) and stromal cells (7AAD- CD45- Ter119- CD31- Sca1+ CD51+) were FACS sorted. Sorted populations from bone marrow and bone fraction were pooled together and counted. An input of 17,000 cells was used for droplet based single cell RNA sequencing.

Single cell library construction and sequencing

Single cells were encapsulated for cDNA synthesis and barcoded using the Chromium Single Cell 3′ Reagent Kit v3 (10X Genomics), followed by library construction according to the manufacturer's recommendations. Sequencing was performed on the NovaSeq 6000 platform (Illumina), paired-end mode, at a sequencing depth of $\geq$ 45,000 reads/cell, followed by computational alignment using CellRanger (v 3.0.2, 10x Genomics).

Single cell RNA sequencing data analysis

Seurat (v 3.1.0) was used for high level analysis of the scRNA-seq dataset (Satija et al., 2015). Unless otherwise specified, default parameters were used. Cells expressing high levels of mitochondrial genes (> 5%) and exhibiting a high ratio of counts over features (> 6) were filtered, since these were considered low viability cells and multiplets, respectively. Cells with a library complexity of less than 200 features were considered empty droplets and hence excluded. The remaining cells were used for downstream analysis.

Normalization and principal component analysis (PCA) were performed on the most variable genes (nfeatures = 5,000) for dimensionality reduction. With the linearly uncorrelated principal components (npcs = 40), we performed unsupervised clustering using a shared nearest neighbor (SNN) modularity optimization-based clustering algorithm (resolution = 0.3). Visualization was performed by nonlinear dimension reduction using the Uniform Manifold Approximation and Projection (UMAP, McInnes et al., 2018).

Endothelial cells were subsetted based on *Cdh5* expression (normalized expression level > 0) and reclustered (resolution = 0.3). Dimensionality reduction was performed as described above. Similarly, stromal cells were subsetted based on the positive expression of *Prrx1* (normalized expression level > 0) and reclustered (resolution = 0.3).

For GSEA analysis marker genes were selected at a significance level of 0.05. Features were pre-ranked using a direction weighted p value. Upregulated markers were assigned a positive p value and downregulated markers a negative value. Murine gene symbols were converted into human gene symbols using the biomaRt package (v 2.42.0) and subsequently subjected to GSEA analysis as described (version 4.0.3; Subramanian et al., 2005).

Pseudotime analysis

Pseudotime analysis is based on Monocle (version 2.12.0; Trapnell et al., 2014). As input for Monocle, we used the 1000 most relevant genes identified by Monocle's unsupervised feature selection approach (dpFeature). Other parameters were based on default values.

FACS of murine niche cells

To define and determine the frequencies of murine niche cells, collagenased bone fraction cell suspensions were obtained as previously described (Zambetti et al., 2016) and stained with the following antibodies: anti-CD45.2 (clone 104, 1:100), anti-Ter119 (clone TER-119, 1:25), anti-CD144 (clone BV13, 1:200), anti-CD51 (clone RMV-7, 1:50), anti-Sca1 (clone D7, 1:50) all from Biolegend, anti-CD140α (clone APA5, 1:100) from eBioscience, and anti-CD31 (clone MEC 13.3, 1:100) from BD Biosciences. Alexa Fluor 488-conjugated Streptavidin (1:100, Invitrogen) was used to detect cells marked by biotin anti-CD51 antibody. 7-Amino-Actinomycin D viability dye (7-AAD, 1:100, Beckman Coulter) was used to distinguish between living and dead cells. For bulk-RNASeq, cells were directly sorted into 800μl Trizol (Ambion) for RNA isolation.

Immunofluorescence imaging of murine sternum

Sterna of *VE-Cadherin-Cre;LoxP-tdTomato* mice were fixed in 4% paraformaldehyde for 24 hours at room temperature, subsequently incubated in 30% sucrose in PBS at 4°C, overnight and embedded in OCT. 6 μm sections were obtained and placed on Superfrost slides (Fisher Scientific). Sections were mounted using ProLong Gold Antifade Mountant with DAPI (Invitrogen). Images were acquired with a Leica TCS SP5 confocal microscope.

Murine stromal cell flow cytometry analysis

Stromal cells derived from BM of 3 week-old *VE-Cadherin-Cre;LoxP-tdTomato* mice were cultured until confluent and stained with the following antibodies for flow cytometry analysis: anti-CD45.2 (clone 104, 1:100), anti-CD144 (clone BV13, 1:200) from Biolegend, anti-CD31 (clone MEC 13.3, 1:100), anti-CD44 (clone IM7, 1:300) from BD Biosciences, and anti-CD29 (clone HMb1-1, 1:100) from eBioscience.

ECFC and HUVEC RNA extraction and gene expression analyses

Total RNA extraction was performed using NucleoSpin RNA II (Machery Nagel) or TriZOL Reagent (Invitrogen) and chloroform according to manufacturer's instructions. RNA purity and quantity were assessed using Nanodrop spectrometric analysis. All relative absorbances (A260/280 and A260/230) were > 2.0. RNA integrity was assessed on a 1% Agarose gel. Up to 2 μg of RNA were retrotranscribed using RevertAid First Strand cDNA Synthesis Kits (Fisher Scientific), and real-time reverse transcription-PCR experiments were performed using SYBR Green (Bio-Rad) and a Bio-Rad CFX Connect device.

HUVEC flow cytometry analyses

Prior to analysis, HUVECs were either treated with vehicle-control (milli Q water) or stimulated with IL-33 (10 ng/ml or 100 ng/ml, ProSpec), and/ or with TGF-β1 (10 ng/ml, R&D Systems) for 96 hours in ECM without ECGF. Culture medium was refreshed daily during stimulation. HUVECs were stained with the following antibodies using optimized dilutions: CD144 (clone 55-7H1, 1:50) and CD34 (clone 8G12, 1:50) from BD Biosciences, CD31 (clone WM59, 1:50), CD271 (clone ME20.4, 1:100), and CD44 (clone IM7, 1:50) all from Biolegend, and CD90 (clone eBio5E10, 1:100) from eBioscience.

Accordingly, cells were also incubated with appropriate mouse IgG1, kappa isotype controls: APC/Cy7, FITC, PE, PE/Cy7, all from Biolegend, V450 from BD Biosciences, and APC from eBioscience. Flow-cytometric analysis was performed using a BD LSRII (BD Biosciences) and data were analyzed using FlowJo (Tree Star Inc).

HUVEC endothelial barrier function assays

Endothelial barrier function analysis was performed using impedance-based cell monitoring using electric cell-substrate impedance sensing system (ECIS Zθ, Applied Biophysics). HUVECs were seeded on 1% gelatin-coated ECIS arrays each containing 8 wells with 10 gold electrodes 2 per well (8W10E PET, Applied Biophysics). The cell seeding density was estimated ~50,000cells/cm2.

Two assay protocols were performed. First, after stabilization of the chip, HUVECs were seeded for at least 24h in complete EBM2 growth medium containing 10% FBS. Then, the medium was replaced by EBM2:Alpha-MEM (containing 10% FBS) 1:9, supplemented with either recombinant IL-33 (100 ng/ml) or control vehicle (milli Q water). Stabilization of the barrier was monitored in real time over 40 hours. Multiple frequency/time (MFT) mode was used for the real-time assessment of the barrier and monolayer confluence. Mathematical modeling of cell-matrix contacts (alpha) was performed as previously described (Szulcek et al., 2014). An

additional assessment of barrier function was performed. Briefly, subconfluent HUVECs were stimulated with IL-33 (100 ng/ml) or control vehicle in EBM2 growth medium containing 10% FBS for 72 hours. Subsequently, cells were dissociated, centrifuged and resuspended in EBM2:Alpha-MEM (containing 10% FBS) 1:9, and seeded in precoated ECIS chips. Impedance measurements were performed for 70 hours as described above.

Immunofluorescent labeling of endothelial cells

For immunofluorescent labeling of ECFCs and HUVECs *in vitro*, cells grown on coverslips were fixed with 4% formaldehyde for 30 minutes at room temperature, washed with glycine for 5 minutes, permeabilized with 0.2% Triton X-100 and blocked in PBS containing 5% bovine serum albumin (BSA) for one hour. Next, the cells were incubated overnight at 4°C in blocking solution containing primary antibody with gentle shaking. Next day, the cells were washed 5 times in washing buffer (PBS containing 0.05% Tween-20 and 1% BSA) and incubated with the following secondary antibodies: FITC goat anti-mouse IgG (Jackson ImmunoResearch Labs), Alexa Fluor Plus 555 goat anti-rabbit IgG (Thermo Fisher Scientific) and Cy3 goat anti-mouse IgG (1:200, Jackson ImmunoResearch Labs) in PBS with 0.5% BSA for one hour. Finally, the cells were washed 5 times in washing buffer and mounted in Prolong Gold containing DAPI (Invitrogen). After careful drying, the preparations were imaged with a Leica SP5 confocal scanning laser microscope. The following antibodies were used for immunofluorescent staining: VE-Cadherin (Cell Signaling, 1:100), Fibronectin (Sigma-Aldrich, 1:400), apha-SMA (Sigma-Aldrich).

Osteogenic, adipogenic, and chondrogenic differentiation assays

For osteogenic differentiation, 3×10^3 stromal cells/cm^2 were cultured in osteogenic induction medium (High glucose DMEM containing glutamax (Invitrogen) supplemented with 10% FCS, 10 mM glycerophosphate (Sigma-Aldrich), 0.1 μM Dexamethasone (Sigma-Aldrich), and 0.1 mM Vitamin-C (Sigma-Aldrich)). Medium was refreshed every 3-4 days at 37°C and 5% CO_2. At end of culture (day 17-21 depending on macroscrope observation of mineralization or cell sheets detaching from outer periphery of well), cells were fixed in 70% ethanol (vol/vol) at 4°C for 1 hour, and after consecutive PBS washes, were stained for 10-20 minutes with an alizarin Red S solution (saturated Alizarin Red S (Sigma-Aldrich) in demineralized water adjusted to pH 4.2 using 0.5% ammonium hydroxide).

For adipogenic differentiation, 2.1×10^4 stromal cells/cm^2 were cultured in adipogenic induction medium (High glucose DMEM containing glutamax supplemented with 10% FCS, 1μm Dexamethasone, 0.2 mM indomethacin (Sigma-Aldrich), 0.01 mg/ml insulin (Sigma-Aldrich), 0.5 mM 3 iso-butyl-l-methyl-xanthine (Sigma-Aldrich). Medium was refreshed every 3-4 days at 37°C and 5% CO_2. At end of culture (day 14), cells were fixed in 4% PFA/PBS for 10 minutes, and stained for 10-15 minutes with an Oil red-O solution (0.5% w/v Oil-red O (in 2-propanol; Sigma-Aldrich)) followed by rinsing in distilled water.

For chondrogenic differentiation, $2x10^5$ stromal cells were suspended in complete chondrogenic induction medium (High glucose DMEM containing glutamax supplemented with 1mM Sodium pyruvate (Invitrogen), 40μg/ml Proline (Sigma-Aldrich), 1:100v/v insulin-transferrin-selenium (BD Biosciences), 10 ng/ml TGF-β3 (R&D Systems), 100 nM dexamethasone (Sigma-Aldrich)) in 15ml polypropylene tubes then centrifuged at 200 g for 8 minutes. Medium was refreshed every 3-4 days at 37°C and 5% CO_2. At end of culture (day 21), cell pellets were fixed in 4% PFA/PBS for one hour, embedded in liquid paraffin wax, and cut into 5 μm sections. After deparaffinization, sections were stained for 5 minutes with a thionin solution (0.04% thionin (Sigma-Aldrich) in 0.01M aqueous sodium acetate pH 4.5) or 10 minutes with Toluidine Blue solution (0.4% toluidine blue (Sigma-Aldrich) in 0.17M aqueous sodium acetate pH 4.0).

Osteogenic differentiation assays in endothelial cells

For mineralization assays, 5×10^4 ECFCs or HUVECs were seeded into 48-well plates and incubated in growth medium in the presence of IL-33 (10, 100 ng/ml) or mQ vehicle-control for 5 days. Subsequently, the medium was replaced by osteogenic medium (EBM2:alpha mem 1:9 containing 10% FBS) supplemented with 10^{-8} mol/L dexamethasone, 0.2 mmol/L ascorbic acid and 10 mmol/L β-glycerolphosphate for 21 days. The medium was refreshed every 4 days. Afterward cells were washed twice with PBS and fixed with 3.7% formaldehyde for 5 minutes, prior to perform Alizarin Red as previously described (Sánchez-Duffhues et al., 2015). Precipitates originated from 3 independent ARS assays were dissolved using 10% cetylpyridinium chloride and absorbance was measured at 545 nm. In addition, *von Kossa* staining was performed by incubating the fixed cells in a 1% silver nitrate solution for 1 hour under ultraviolet light. Next, the cells were rinsed twice with distilled water and washed with 5% sodium thiosulfate for 5 minutes. After washing twice with distilled water, counterstaining was performed with Nuclear Fast Red solution (Sigma-Aldrich). Representative pictures were obtained using a Leica DMIL LED microscope with 10 times magnification.

In order to measure alkaline phosphatase enzymatic activity, ECFCs or HUVECs were seeded as aforementioned, and incubated for one week in growth medium (EBM2, Lonza) in the presence of IL-33 (10, 100 ng/ml) or mQ vehicle-control for 7 days. For quantification, cells were washed twice with phosphate buffered saline (PBS) and frozen for 1 hour at −80 C. Next, cells were lysed in ice with Triton X-100 buffer for 1 hour. Lysates were incubated at room temperature with a 4-Nitrophenyl phosphate disodium salt solution (PNPP) solution till it turned yellow and absorbance was measured at 405 nm.

QUANTIFICATION AND STATISTICAL ANALYSIS

Statistical analyses were performed using Prism 8 (GraphPad Software) and SPSS 24 (IBM). Unless otherwise specified, unpaired, 2-tailed Student's t test (single test for comparison of 2 means) or 1-way ANOVA followed by Bonferroni correction for multiple comparisons were used to evaluate statistical significance, defined as $p < 0.05$. All results in bar graphs are means ± SEMs, if not otherwise specified. The number of replicates is indicated in the figure legends, including the number of independent experiments.